U.PORTO

MESTRADO ONCOLOGIA

ESPECIALIDADE EM ONCOLOGIA LABORATORIAL

Functional impact of loss of the intestinal stem cell marker MEX3A in chromosomal instability (CIN)+ colorectal cancer tumoroids

Morgana De Vargas Russel

M

2022

U.PORTO

Morgana De Vargas Russel. Functional impact of loss of the intestinal stem cell marker MEX3A in chromosomal instability (CIN)+ colorectal cancer tumoroids

M.ICBAS.2022

Functional impact of loss of the intestinal stem cell marker MEX3A in chromosomal instability (CIN)+ colorectal cancer tumoroids

Morgana De Vargas Russel

INSTITUTO DE CIÊNCIAS BIOMÉDICAS ABEL SALAZAR

MORGANA DE VARGAS RUSSEL

FUNCTIONAL IMPACT OF LOSS OF THE INTESTINAL STEM CELL MARKER MEX3A IN CHROMOSOMAL INSTABILITY (CIN)+ COLORECTAL CANCER TUMOROIDS

Dissertação de Candidatura ao grau de Mestre em Oncologia – especialização em Oncologia Laboratorial – submetida ao Instituto de Ciências Biomédicas Abel Salazar da Universidade do Porto.

Orientador: **Doutor Bruno Miguel Correia Pereira**

Categoria – Junior Researcher

Afiliação – Differentiation and Cancer Group, Instituto de Investigação e Inovação em Saúde/ Instituto de Patologia e Imunologia Molecular da Universidade do Porto (i3S/IPATIMUP).

Co-orientador: **Doutor Carlos Alberto da Silva Conde**

Categoria – Associate Researcher

Afiliação – Cell Division & Genomic Stability, Instituto de Investigação e Inovação em Saúde/ Instituto de Biologia Molecular e Celular (i3S/IBMC).

Financial Support

FCT Fundação para a Ciência e a Tecnologia
MINISTÉRIO DA CIÊNCIA, TECNOLOGIA E ENSINO SUPERIOR

This work was funded by Fundação para a Ciência e Tecnologia (FCT) with the grant PTDC/BIA-CEL/0456/2021. This work has also been supported by the following entities: Portuguese funds through FCT in the framework of the project "Institute for Research and Innovation in Health Sciences" (POCI-01-0145-FEDER-007274); NORTE-01-0145-FEDER-000029, Norte Portugal Regional Programme (NORTE 2020), under the PORTUGAL 2020 Partnership Agreement, through the European Regional Development Fund (ERDF); FEDER - Fundo Europeu de Desenvolvimento Regional funds through the COMPETE 2020 - Operational Programme for Competitiveness and Internationalisation (POCI), Portugal 2020.

A ti pai reservo toda a minha saudade, amor, respeito e admiração eterna.
Obrigada por ter dedicado a vida a proporcionar o melhor para a nossa família.
Obrigada por me apoiar, incentivar e me dar toda a estrutura para voar tão longe.
Dedico este trabalho a tua luta contra esta doença que te levou tão cedo de nós.

Te amo mais que o infinito
Da tua maninha, Moi

Acknowledgments

Após 2 anos de Mestrado termina mais um ciclo na minha vida. Neste momento me sinto feliz e agradecida por todos que fizeram parte deste percurso.

Em primeiro lugar, gostaria de agradecer o meu orientador Bruno Pereira, por todo o suporte, disponibilidade e conhecimentos que você me passou. Sou muito grata pelas oportunidades que você me deu de realizar a tese no grupo, como também o estágio curricular do mestrado. Obrigada por ter sido tão paciente comigo e por sempre me incentivar a tentar novamente quando algo correu mau.

Um agradecimento especial à Raquel Almeida, líder do grupo *Differentiation & Cancer*, por ter me aceitado no grupo durante este período. Aos restantes membros, agradeço por todo apoio e ensinamentos que vocês partilharam comigo. Em especial à Rita Silva, que me ensinou muitos "hacks" para facilitar a vida em alguns protocolos, além de ter encontrado soluções em momentos que achei que estava tudo perdido. À Vanessa Machado que também foi parte essencial no meu percurso. E meu muito obrigada à Beatriz Almeida, por ser a aluna de mestrado com quem partilhei o ano e (as vezes) o desespero haha, pelos cafés e os chocolates na cantina.

Além disso, gostaria de agradecer ao meu co-orientador Carlos Conde, por ter aceitado me coorientar e fazer parte deste projeto em parceria com grupo *Cell Division & Genomic Stability*. À Ana Pinto por ter me transmitido seus conhecimentos sobre *Live Cell Imaging* e por ter tornado estes momentos mais leves e descontraídos, sempre me incentivando com o seu bom humor.

Agradeço também ao corpo docente do Mestrado em Oncologia do ICBAS-IPO, em especial a Diretora do Mestrado professora Carmen Jerónimo por todo o suporte durante este percurso.

Aos queridos amigos que fiz ao longo do curso Ana Vilarinho, Rita Santos, João Conde e Taynah: eu adoro vocês! Tudo foi mais fácil tendo vocês por perto, obrigada por marcarem este percurso e terem tornado o Porto o meu lar, já sinto falta da nossa convivência diária e dos nossos jantares.

A lista de agradecimentos a amigos e familiares ainda seria muito longa, mas deixo aqui o meu obrigada a todos que fizeram parte de fato desta jornada. Em especial à Letícia Campos e a Agnes Rigas.

Por fim, o maior agradecimento desta tese é sem dúvidas à minha família. Como disse a escritora Ruth Manus em um dos seus livros “obrigada por me darem a chance rara, o quase luxo, de apenas viver. Porque todo o resto vocês fizeram por mim”.

À minha mãe, obrigada por tudo que faz e abdica por mim. Obrigada por sempre me incentivar e dar asas para traçar o meu próprio caminho. Por ter me criado do jeito que sou: teimosa e persistente, sem estas características com certeza não teria chegado até aqui. Ao meu irmão Pedro, obrigada por ser o meu melhor amigo e por estar aqui para me amparar, me escutar, me fazer rir e até para brigar. Amo muito vocês dois e não vejo a hora de no vermos novamente no Brasil em breve.

Ao meu namorado Gustavo Rotini, com quem divido a vida há quase 3 anos, obrigada por estar sempre ao meu lado. Obrigada por ter torcido tanto quanto eu e com todas as forças para que este projeto desse certo. Por ter zelado por mim todos os dias que fiquei até tarde escrevendo e você me fazendo companhia. Obrigada por ser o melhor namorado e designer do mundo que me ajudou na formatação desta tese. Te amo minha vida. Também agradeço a família do Gustavo, por ser minha segunda família durante estes últimos anos e estarem sempre me incentivando.

À minha amada vó Elzoir, que infelizmente partiu durante a escrita desta tese, espero que de onde a senhora estiver esteja em paz, feliz e orgulhosa da tua neta favorita. Sou eternamente grata a senhora por ter me apoiado e me proporcionado a chance de há 5 anos me mudar para Portugal em busca dos meus sonhos.

Ao meu pai, a quem não tenho palavras suficientes para descrever o meu amor. Obrigada por ser a minha base, por ter impactado tanto em quem eu sou como pessoa. Por ter me instigado a amar ciências quando criança, por me incentivar a ser curiosa e me questionar sobre as coisas.

Abstract

Colorectal cancer is the third cause of cancer-related deaths worldwide. The colorectal carcinogenesis process leads to a heterogeneous disease resulting from the accumulation of several mutations. RNA-binding proteins (RBPs) are reported to be essential in post-transcriptional events and crucial to dynamically regulate gene expression. Their dysregulation can cause several human pathologies, including cancer. In this context, we have been studying the RBP MEX3A that is involved in intestinal homeostasis by regulating LGR5+ intestinal stem cells (ISCs) identity, but also overexpressed in 80% of human colorectal cancer (CRC) cases. However, the functional impact of MEX3A in colorectal carcinogenesis still needs to be addressed in detail. Given its important role for ISC maintenance, we hypothesized that MEX3A might contribute to tumor cell heterogeneity in a context of chromosomal instability (CIN), the most frequent type of genomic instability observed in CRC. Hence, our objective in this work was to study the putative impact of loss of MEX3A in the colorectal carcinogenesis process at different stages of the disease.

For this, we established two complementary study models: 1) a murine CRC model (early stage) with baseline MEX3A downregulation in which a p53 knockout (KO) was created in order to induce CIN; 2) a human CRC model (late stage) in which a MEX3A KO was introduced. Gene editing was performed by CRISPR-Cas9 system and the models characterized in terms of expression profile for specific cell lineage markers and concerning mitotic fidelity by live-cell imaging.

In the characterization of CRC mouse models, we found that the reduced expression of *Mex3a* decreases tumor burden and alters tumoroids growth and differentiation patterns. Simultaneously, by treating these tumoroids with a PPARγ-selective agonist, we observed the impact of increased PPARγ expression over *Lgr5* expression, particularly in a background of reduced MEX3A expression, indicating loss of stem cell potential. The characterization of human CRC tumoroids, which were shown to mimic primary tumor tissue, reinforced the correlation in expression profile between these markers. The establishment of a human tumoroid line with MEX3A KO provided functional evidence of the role of MEX3A in directly regulating LGR5 expression and the PPARγ pathway. In this context, we also found that cells positive for PPARγ showed increased p53 expression, which might have implications for the level of genomic instability in cells. By performing live-

cell imaging, we obtained preliminary results showing a putative attenuation of the CIN phenotype upon MEX3A KO. However, this correlation needs to be further explored.

Our data elucidates the importance of understanding the effects of MEX3A in colorectal carcinogenesis since it highlights the possibility that this RBP may be involved in intratumoral heterogeneity, leading to poor clinical prognostics. We speculate that MEX3A could be a potential therapeutic target for CRC.

Keywords: Colorectal cancer, Tumoroids, Stem cell, Chromosomal instability, MEX3A, p53

Resumo

O cancro colorretal é a terceira causa de mortes relacionadas com cancro em todo o mundo. O modelo de carcinogénese colorretal é caracterizado por ser um processo heterogéneo resultante da acumulação de diversas mutações. As proteínas de ligação ao ARN (RBPs) são fundamentais em eventos pós-transcricionais e cruciais para a regulação da expressão génica. A alteração destas proteínas pode dar origem a diversas patologias humanas, incluindo o cancro. Neste contexto, temos estudado a RBP MEX3A que está envolvida na manutenção da homeostasia intestinal através da regulação da identidade das células estaminais intestinais (ISCs) LGR5+, mas também sobre-expressa em 80% dos casos de cancro colorretal (CRC) humano. No entanto, o impacto funcional de MEX3A na carcinogénese colorretal ainda precisa de ser aprofundado. Assim, dado o seu importante papel na manutenção das ISCs, levantamos a hipótese de que o MEX3A pode contribuir para a heterogeneidade tumoral em contexto de instabilidade cromossómica (CIN), o mais frequente tipo de instabilidade genómica observada no CRC. Assim, o nosso objetivo neste trabalho foi estudar o impacto funcional da perda de MEX3A no processo de carcinogénese colorretal em diferentes estadios da doença.

Para isso, estabelecemos dois modelos de estudo complementares: 1) um modelo de ratinho com CRC (estadio inicial) com diminuição de MEX3A basal no qual foi introduzido uma alteração (KO) da p53 para induzir o aumento de CIN; 2) um modelo humano de CRC (estadio avançado) no qual foi introduzido um KO para MEX3A. A edição genómica destes modelos foi realizada através do sistema de CRISPR-Cas9 e estes foram caracterizados em termos de perfil de expressão para marcadores de linhagens celulares específicas e classificados quanto à fidelidade mitótica por técnicas de microscopia de *live-cell imaging.*

Na caracterização de modelos de ratinhos com CRC, observamos que a expressão reduzida de *Mex3a* diminui a carga tumoral e altera os padrões de crescimento e diferenciação dos tumoróides. Simultaneamente, ao tratar esses tumoróides com um agonista seletivo da via PPARγ, observamos o impacto da sobre-expressão de PPARγ sobre *Lgr5*, em especial no modelo com expressão reduzida de MEX3A, sugerindo uma perda de potencial estaminal. Para além disso, a caracterização de tumoróides de CRC humanos, capazes de mimetizarem o tecido tumoral primário, reforçou a correlação entre o perfil de expressão destes marcadores. O estabelecimento de uma linha de tumoróide humana com KO MEX3A forneceu evidências funcionais do papel de MEX3A na regulação

direta da expressão de LGR5 e da via PPARγ. Nesse contexto, também observamos que células positivas para PPARγ apresentaram um aumento da expressão de p53, o que pode ter implicações no nível de instabilidade genómica nas células. Ao realizar a técnica de *live-cell imaging*, foi possível obter resultados preliminares quanto a uma provável diminuição do fenótipo CIN nos modelos KO para MEX3A. No entanto, esta correlação precisará de ser mais aprofundada.

Os resultados obtidos neste trabalho reforçam a importância de compreender os efeitos de MEX3A na carcinogénese do cancro colorretal, pois destacam a possibilidade de que esta RBP possa estar envolvida na heterogeneidade intratumoral, associando-se a um pior prognóstico. Especulamos que a RBP MEX3A possa ser um potencial alvo terapêutico no contexto do CRC.

Termos-chave: Cancro colorretal, Tumoróides, Células estaminais, Instabilidade cromossómica, MEX3A, p53

Table of contents

Acknowledgments ..... **VII**

Abstract ..... **X**

Resumo ..... **XII**

Abbreviations ..... **XVII**

Figures Index ..... **XIX**

Tables Index ..... **XXI**

Chapter 1 | Introduction **1**

1.1. Intestinal Biology **1**

1.1.1. Intestinal epithelial homeostasis **2**

1.1.2. Intestinal stem cells (ISCs) identity **2**

1.1.3. Intestinal epithelium self-renewal mechanisms **3**

1.2. Colorectal cancer **5**

1.2.1. Colorectal carcinogenesis **6**

1.2.2. Stem cells as cells of origin of CRC **8**

1.2.3. CRC mouse models **9**

1.2.4. CRC-derived organoids – tumoroid cultures **10**

1.3. CRISPR/Cas9 technology in tumoroids **11**

1.4. RNA-binding proteins **12**

1.4.1. MEX-3 family of RNA-binding proteins **14**

1.4.2. MEX3A protein **15**

1.4.3. The role of MEX3A protein in different cancer types **16**

Chapter 2 | Objectives **18**

Chapter 3 | Material and methods **19**

3.1. Animal models **19**

3.2. Human samples **19**

3.3. Conditioned media production for organoid culture 20
3.4. Organoid culture establishment and maintenance 20
3.5. Genome editing by CRISPR-Cas9 technology 21
3.6. Tumoroid transfection 23
3.6.1. Tumoroid transfection for *Trp53* KO in mouse tumoroids 23
3.6.2 Tumoroid transfection for *MEX3A* KO in human tumoroids 24
3.7. Organoid live cell imaging 24
3.8. Protein extraction and quantification 24
3.9. Western blot analysis 25
3.10. RNA extraction and quantitative real-time PCR 26
3.11. Histochemical procedures 26
3.12. Immunohistochemistry (IHC) 27
3.13. mRNA *in situ* hybridization (ISH) 28
3.14. Statistical analysis 29
Chapter 4 | Results 30
4.1. Establishment of $Apc^{+/F}$;$Kras^{+/G12D}$;$Fabpl^{+/Cre}$;$Mex3a^{+/-}$ mouse-derived CRC tumoroids 30
4.2. $Apc^{+/F}$;$Kras^{+/G12D}$;$Fabpl^{+/Cre}$;$Mex3a^{+/-}$ mouse-derived CRC tumoroids show increased sensitivity to PPARγ pathway activation 31
4.3. Functional evaluation of sgRNAs for *Trp53* KO by CRISPR-Cas9 technology 33
4.4. Establishment of *Trp53* KO CRC mouse tumoroids 36
4.5. Generation of MEX3A KO human tumoroids by CRISPR-Cas9 technology 38
4.5.1. Establishment and characterization of human-derived CRC tumoroids 38
4.5.2. Establishment of MEX3A KO tumoroids 43
4.5.3. Characterization of MEX3A KO tumoroids 45
Chapter 5 | Discussion 48

Chapter 6 | Future perspectives and concluding remarks 53

References 54

Appendix A | List of primers and antibodies used in this study..... 65

Abbreviations

ANGPTL4 – Angiopoietin-like protein 4

APC – Adenomatous polyposis coli

ASCL2 – Achaete scute-like 2

AXIN – Axin-related protein

BMI1 – B cell-specific Moloney murine leukemia virus integration site 1

CBC – Crypt base columnar

CIN – Chromosomal instability

CK1 – Casein kinase 1

CK20 – Cytokeratin- 20

CRC – Colorectal cancer

CRISPR – Clustered regularly interspaced short palindromic repeats

CSC – Cancer Stem Cells

DSBs – DNA double-stranded breaks

EGF – Epidermal Growth Factor

FZD – Frizzled membrane receptor

GSK3 – Glycogen synthase kinase 3

IEC – Intestinal epithelial cell

ISC – Intestinal stem cell

ITH – intratumoral heterogeneity

KRAS – Kirsten rat sarcoma viral oncogene homolog

KO – Knockout

LEF – Lymphoid enhancer factor

LGR5 – Leucine-rich repeat-containing G-protein coupled receptor 5

LRIG1 – Leucine-rich repeats and immunoglobulin-like domains 1

LRP5 – Low-density lipoprotein receptor-related protein 5

MEX3A – Mex-3 RNA Binding Family Member A

MMR – DNA Mismatch repair

MRE – MEX-3 recognition element

MSI – Microsatellite instability

NOG – Noggin

PAM – Protospacer Adjacent Motif

Pcna – Proliferating Cell Nuclear Antigen

PPAR – Peroxisome proliferator-activated receptor

RBD – RNA-binding domain

RBP – RNA-binding protein

RNP – Ribonucleoprotein;

RRM – RNA recognition motif

RSPO – R-spondin

SI – Small intestine

TA – Transit-amplifying

TCF – T cell factor

Figures Index

Figure 1 | Intestinal epithelial cells structure and organization 1

Figure 2 | The canonical Wnt signaling 4

Figure 3 | Distribution of cases and deaths for the top 10 most common cancers in 2020..5

Figure 4 | Adenoma-carcinoma model and CIN onset in CRC 7

Figure 5 | The Cas9 protein 12

Figure 6 | RNA-binding proteins regulating RNA life cycle 12

Figure 7 | RNA-binding protein acting on RNA 13

Figure 8 | The first Mex3a knockout mice 15

Figure 9 |The pSpCas9(BB)-2A-GFP (PX458) plasmid map. 22

Figure 10 | Typical CRC lesions present in the colon of *Apc*$^{+/F}$;*Kras*$^{+/G12D}$;*Fabpl*$^{+/Cre}$ *and* *Apc*$^{+/F}$;*Kras*$^{+/G12D}$;*Fabpl*$^{+/Cre}$;*Mex3a*$^{+/-}$ mice 30

Figure 11 | *Apc*$^{+/F}$;*Kras*$^{+/G12D}$;*Fabpl*$^{+/Cre}$ *and Apc*$^{+/F}$;*Kras*$^{+/G12D}$;*Fabpl*$^{+/Cre}$;*Mex3a*$^{+/-}$ tumoroids after 7 days of culture 31

Figure 12 | *Apc*$^{+/F}$;*Kras*$^{+/G12D}$;*Fabpl*$^{+/Cre}$ *and Apc*$^{+/F}$;*Kras*$^{+/G12D}$;*Fabpl*$^{+/Cre}$;*Mex3a*$^{+/-}$ tumoroids response to PPARγ agonist treatment 32

Figure 13 | Gene expression analyses by quantitative real-time PCR 33

Figure 14 | Sanger sequencing electropherograms for the sgRNAs insertion site in PX458 vector 34

Figure 15 | Validation of sgRNAs against p53 in L-cells 35

Figure 16 | Validation of the transfection protocol in *Apc*$^{+/F}$;*Kras*$^{+/G12D}$;*Fabpl*$^{+/Cre}$ tumoroid. 36

Figure 17 | Tumoroids *Apc*$^{+/F}$;*Kras*$^{+/G12D}$;*Fabpl*$^{+/Cre}$;*Mex3*$^{+/-}$ *and Apc*$^{+/F}$;*Kras*$^{+/G12D}$;*Fabpl*$^{+/Cre}$ growing after transfection and Nutlin-3a treatment..... 37

Figure 18 | Characterization of normal colon and CRC tissue of patient 007 and respective tumoroids..... 40

Figure 19 | mRNA ISH for *MEX3A* and *LGR5* in 007N tissue, 007T tissue, 007T Wnt, and 007T without Wnt..... 40

Figure 20 | Correlation of expression patterns for different markers between organoids derived from patient 005 and tumoroids of patients 005 and 010 41

Figure 21 | Correlation of expression patterns for different markers between organoids derived from patient 005N and tumoroids of patients 005 and 010..... 42

Figure 22 | mRNA ISH for *MEX3A* and *LGR5* expression patterns markers between organoids derived from patient 005N and CRC-tumoroids of patients 005, and 010 42

Figure 23 | Expression pattern of MEX3A and PPARγ on organoids and tumoroids of patient 005..... 43

Figure 24 | Schematic view of the establishment of MEX3A KO tumoroids 44

Figure 25 | Characterization of 005T Wnt AE6 tumoroids 45

Figure 26 | Chromosome segregation errors in organoids 46

Tables Index

Table 1 | Designed guides sequences for *Trp53* KO and MEX3A KO and their scores.... 22

Chapter 1 | Introduction

1.1. Intestinal Biology

The human intestinal tract is mainly responsible for digestion, absorption of nutrients, and water uptake. It is the fastest self-renewing tissue in adult mammals, with a complete turnover in 3-5 days in mice and 5-7 days in humans (Barker, 2014). The gut is divided into two anatomical portions with distinctive histology and cell organization: the small intestine (SI) and the colon (Figure 1). The SI is mainly responsible for nutrient absorption and subdivided into the duodenum, jejunum, and ileum. Furthermore, SI has several finger-like protrusions known as villi, projecting into the lumen, responsible for maximizing the absorption area. In each villus, there are at least 6 crypts of Lieberkühn penetrating the submucosa (Clevers, 2013). In contrast, the colon is mostly where water is absorbed and is divided into four parts: ascending, transverse, descending, and sigmoid colon. The colon is characterized by the absence of villi structures and the exhibition of a flat luminal surface (Barker et al., 2008).

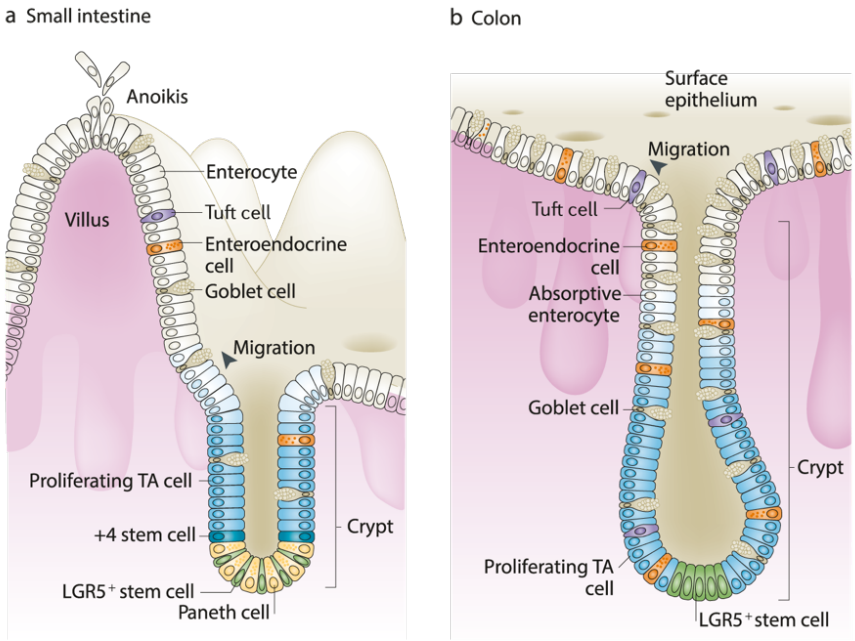

Figure 1 | Intestinal epithelial cells structure and organization. Representative image of the intestinal epithelial cell organization in two distinct anatomical portions. a) Small intestine shows the villus structure and the organization of the crypt, including the presence of Paneth cells. b) Colon shows the absence of villus and differences in proportion of the cell types. Adapted from Barker (2014).

1.1.1. Intestinal epithelial homeostasis

The intestinal tract consists of a single layer of intestinal epithelial cells (IEC) that form a physical barrier composed of specialized cell types responsible for daily protection and processing the dietary nutrients (Hooper & MacPherson, 2010). The IECs comprise four main differentiated cell populations: columnar cells (enterocytes and colonocytes), goblet cells, endocrine cells, and Paneth cells (Simons & Clevers, 2011).

The columnar cells are the most abundant IEC type, responsible for nutrient absorption and transporting. The goblet cells are specifically responsible for the secretion of protective mucigenic granules into the intestinal surface, thus creating a mucus layer that extends ~150μm from the surface to the lumen, essential to safeguard the cells from bacterial penetration (Johansson et al., 2008). The goblet cells are also increased in number in the colonic mucosa compared to SI. In contrast, the Paneth cells are only found in the crypt bases of the SI. These cells are responsible for producing several proteins, including lysozymes and antimicrobials that help to maintain a balanced microbiota in the crypt-villus. The endocrine cells constitute approximately 1% of all IECs, and are responsible for coordinating certain intestinal functions through hormone secretion. Moreover, the remarkable turnover capacity of the gut mucosa is due to the presence of a resident population of adult intestinal stem cells (ISCs) that divide to produce more ISCs and proliferating transit-amplifying (TA) cells that after several divisions commit into the differentiated cell types previously mentioned (Sato, Van Es, et al., 2011; Van Der Flier & Clevers, 2009; Van Es et al., 2005; VanDussen et al., 2012).

1.1.2. Intestinal stem cells (ISCs) identity

The ISCs maintain the balance between self-renewal and differentiation in the gut mucosa. In the past decades, the identity of ISCs was a matter of intense debate, leading the scientific community to two different schools of thought: the classical model and the stem cell zone model.

The classical model suggests that the ISCs exist in “position +4” relative to the crypt bottom. This theory says that self-renewal and differentiation is regulated by slow cycling cells located directly above the Paneth cells compartment (the first three positions from the bottom) (Potten, 1977). These cells were also considered radiosensitive and capable of retaining DNA labels (Potten et al., 2002). In contrast, the “stem cell zone” model reported that the true ISCs responsible for self-renewal and maintenance of the IECs were the crypt

base columnar (CBC) cells, located between the Paneth cells (Bjerknes & Cheng, 1981; Cheng & Leblond, 1974). In this model, the CBCs cycle every day and are sensitive to radiation-induced damage (Barker et al., 2012). Meanwhile, the field evolved to demonstrate that the two populations of ISCs coexist in the crypts and can in fact interconvert between these different states (Li & Clevers, 2010). Ultimately, it is thought that the CBCs contribute to homeostatic regeneration, whereas '+4' cells constitute quiescent reserve stem cells acting only when there is injury to the mucosa that impairs CBCs function (Takeda et al., 2011).

Unfortunately, for many decades no specific ISC markers were determined. However, with the development of new technologies, such as genetic labeling systems, researchers started to identify new specific ISC markers and describe their putative role. In this perspective, the leucine-rich G protein-coupled receptor 5 (LGR5) was the first stem cell marker identified and remains the most reliable one to date. LGR5+ cells were shown to possess capability for long-term self-renewal and differentiation in the crypt (Barker et al., 2007; Sato et al., 2009). Furthermore, other CBC markers were described, such as Olfactomedin-4 (OLFM4) and Achaete scute-like 2 (ASCL2) (van der Flier, Haegebarth, et al., 2009; van der Flier, van Gijn, et al., 2009). Additionally, at cell "position +4", Leucine-rich repeats and immunoglobulin-like domains 1 (LRIG1), and B cell-specific Moloney murine leukemia virus integration site 1 (BMI1) were also identified (Powell et al., 2012; Sangiorgi & Capecchi, 2008).

1.1.3. Intestinal epithelium self-renewal mechanisms

The intestinal epithelium homeostasis is regulated by signaling pathways that guarantee the equilibrium between ISC proliferation and differentiation in the intestinal crypts. In this perspective, the Wnt/β-catenin signaling pathway plays a vital role (Figure 2) (Zhong et al., 2021).

In mammalian species, the Wnt proteins possess highly conserved cysteine residues with a N-terminal signal peptide for secretion (Willert et al., 2003). To activate the canonical Wnt/β-catenin pathway, a multistep process is required to lead the effector protein β-catenin to play its role in activating transcription of target genes (Schatoff et al., 2017). Overall, without Wnt signals, the β-catenin protein is trapped in a "destruction complex" and targeted for degradation. The "destruction complex" consists of the proteins Axin-related protein (*AXIN)* the tumor suppressor *Adenomatous polyposis coli (APC), casein kinase 1 (CK1),*

and *glycogen synthase kinase 3 (GSK3).* β-catenin is targeted for degradation by CK1 and GSK3-mediated phosphorylation on the N-terminal portion leading to its ubiquitination and posterior proteasome-mediated destruction. Additionally, in the absence of Wnt signals, the T cell factor/lymphoid enhancer factor (TCF/LEF) family of activators is bound by transcriptional repressors, such as Groucho, to ensure the repression of Wnt responsive genes (Clevers, 2006).

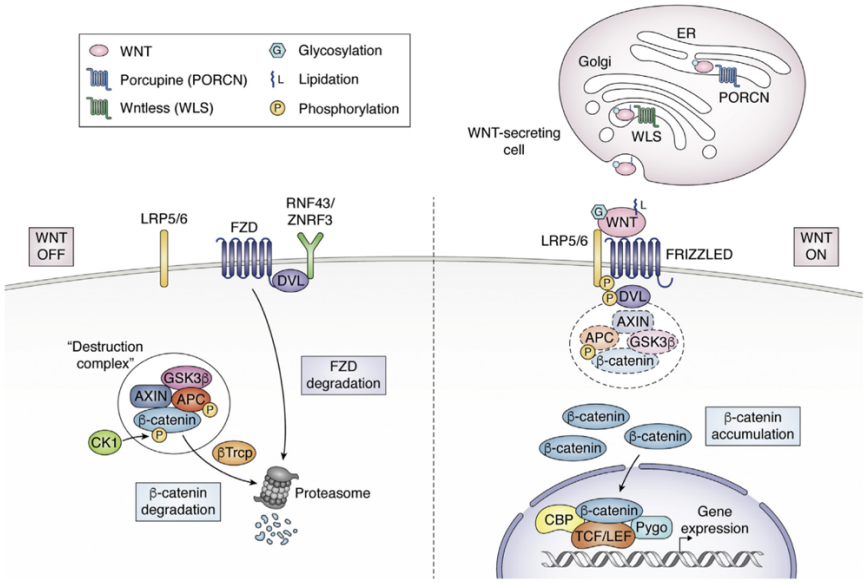

Figure 2 | The canonical Wnt signaling. Schematic representation of Wnt/β-catenin signaling. The left panel shows the absence of Wnt ligands on the FZD receptor and the β-catenin attached to the "destruction complex," targeted for destruction by the proteasome. On the right panel, the canonical Wnt signaling is active by the Wnt signals bounded to FZD/LRP coreceptor complex and their scaffold proteins. The β-catenin is now free to translocate to the nucleus and promote the transcription of Wnt target genes. Adapted from Zhong et al. (2021).

In contrast, to activate the canonical pathway, Wnt ligands bind to seven-pass transmembrane Frizzled (FZD) receptors (Bhanot et al., 1996). After binding, these FZD receptors interact with the low-density lipoprotein receptor-related protein 5 or 6 (LRP5/6), forming a coreceptor complex, thus initiating the membrane recruitment of scaffold proteins such as APC, AXIN and Dishevelled (DVL) and liberating the β-catenin from the "destruction complex." With the complex inactivated, β-catenin is stabilized and translocated into the nucleus. In the nucleus, it acts as transcriptional co-activator, binding to TCF/LEF family transcription factors and leading to expression of Wnt-responsive genes (MacDonald et al., 2009).

Activation of the Wnt/β-catenin pathway promotes stem-like phenotypes, which includes the expression of LGR4/5/6 in ISCs. It is well-known that these proteins act as receptors for the ligand members of the R-spondin (RSPO) family. Thus, when LGR5/RSPO complex is bounded, it acts as a Wnt pathway agonist by neutralizing the membrane E3 ubiquitin-protein ligases ZNRF3 and RNF43, creating a mechanism of negative feedback mediated by these enzymes, removing the Wnt receptors from the cell surface to regulate the Wnt/β-catenin pathway (de Lau et al., 2014; Yan et al., 2017). Nonetheless, abnormal signaling or activation of the Wnt pathway leads to abnormal expression of β-catenin and cancer development in different contexts, most notably colorectal cancer (CRC).

1.2. Colorectal cancer

CRC is a prevalent and aggressive disease that affects both the colon and rectum. Overall, CRC is the third most common cancer type worldwide for both sexes (Figure 3), accounting for 10,6% of new cases in men and 9,4% for women. In addition, according to the last GLOBOCAN analyses, it is the second cancer-related cause of death, with over 935,000 estimated deaths in 2020 (Sung et al., 2021).

The incidence of this cancer differs around the world, with higher incidences in developed countries. From this perspective, CRC showed higher frequency and mortality rates in Eastern Asia, North America, and Europe (Central and Eastern). In addition, there were approximately 10.500 new cases of CRC in Portugal in 2020, making CRC the most frequent and the second most lethal cancer in Portugal for both sexes (Sung et al., 2021).

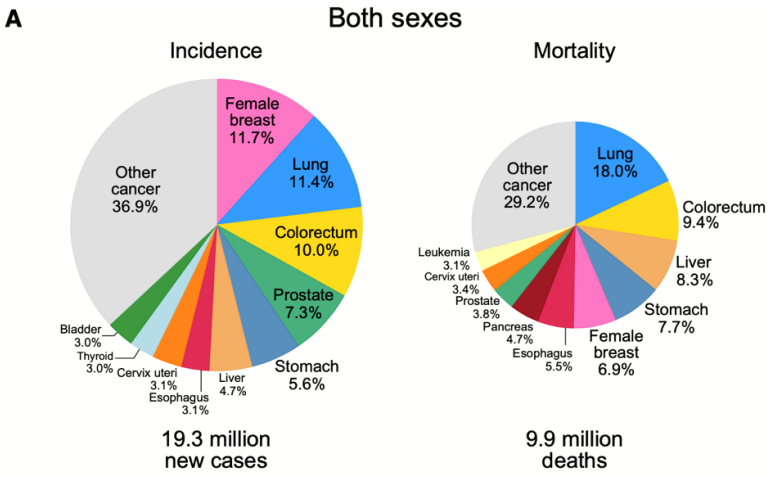

Figure 3 | Distribution of cases and deaths for the top 10 most common cancers in 2020. A representative pie chart showing the proportion of the total number of cancer cases or deaths for both sexes in 2020. Source: GLOBOCAN 2020. Adapted from Sung et al. (2021).

In terms of causes and risk factors for the development of CRC, it is known that age plays a significant role, affecting especially people over 50 years old, while it can occur at any age. In addition, the risk of developing CRC is increased with a family history of CRC, inflammatory bowel disease (IBD), including ulcerative colitis or Crohn's disease, and other syndromes disorders (Amersi et al., 2005; Lauby-Secretan et al., 2018). Furthermore, it appears that there is a relation between the prevalence of CRC and higher levels of the Human Development Index (HDI), which matches to the higher frequency observed in developed countries (Arnold et al., 2017). This relation reflects population lifestyle factors and diets, including the increase in several known risk factors like obesity, alcohol consumption, a poor diet based on processed foods, sedentarism, and tobacco smoking (IARC, 2022).

Nonetheless, the scenario is starting to change in recent years with the implementation of CRC screenings programs as a primary prevention strategy, especially in developed countries. Medical doctors recommend regular screening tests such as colonoscopy for people over 50 or those with familiar history of the disease. Moreover, this exam allows the early detection of benign masses of cells in the form of polyps, usually small and non-symptomatic. However, these polyps can progress to cancer when not picked up in early stages. For this reason, early identification and the removal of precursor lesions are helping to stabilize the incidence of CRC, especially in high-incidence countries. At the same time, more cases of early-onset CRC have been detected (Araghi et al., 2019).

Although there are efforts worldwide to increase primary prevention and awareness of the risk factors, CRC is still a very aggressive cancer with poor prognosis when diagnosed in late stages. The survival rate for patients with CRC depends on the stage of the disease, and it was shown that the 5-year survival rate drops with disease evolution from 90% to 14% when CRC is diagnosed as a localized cancer versus presence of distant metastasis (Mattiuzzi et al., 2019). Overall, this shows how crucial the discovery of new targeted therapies is for patients who will not benefit from existing standard treatments.

1.2.1. Colorectal carcinogenesis

CRC is a heterogeneous disease resulting from acquiring and accumulating multiple genetic mutations and epigenetic alterations (Figure 4). Therefore, most CRC cases are sporadic, but a hereditary component might be present in 15-30% of the cases (Mundade et al., 2014). The classical genetic model for CRC was described in the 1990s as a gradual

process that most often begins with the inactivation of the *APC* gene (70 to 80% of cases), creating structures named adenomatous polyps in the colonic mucosa, which by accumulation of other mutations such as on the oncogene *KRAS* and inactivation of the tumor suppressor gene *TP53*, leads to adenocarcinoma development (Fearon & Vogelstein, 1990). The serrated adenocarcinoma pathway is a recently described subset of CRC that accounts for about 10% of all CRCs and follows an alternative pathway in which serrated polyps replace the traditional adenoma as the precursor lesion to CRC. Serrated polyps form a heterogeneous group of colorectal lesions that includes hyperplastic polyps (HPs), sessile serrated adenoma (SSA), traditional serrated adenoma (TSA) and mixed polyps (Mäkinen, 2007). Genetically, serrated polyps also exhibit a distinct pattern, with *KRAS* and *BRAF* mutations having an important contribution to their development (Leggett & Whitehall, 2010).

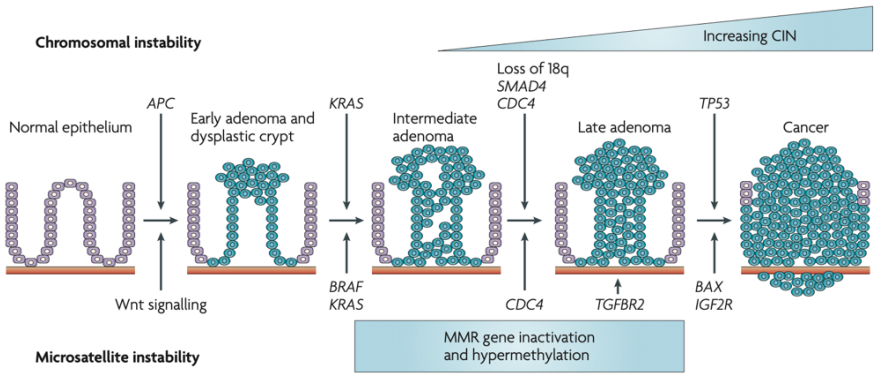

Figure 4 | Adenoma-carcinoma model and CIN onset in CRC. Schematic overview of the adenoma-carcinoma process in CRC showing the initial loss of *APC* and the progressively acquired mutations in genes such as *KRAS, SMAD4, TP53,* and others. This increased the CIN+ phenotype and led to clinicopathological changes with the development of a tumor. Adapted from Walther et al. (2009).

A certain level of genomic instability is associated with CRC development, and is now considered a hallmark of colorectal carcinogenesis. Three major molecular pathways are well-described for CRC development: microsatellite instability (MSI), CpG island methylator phenotype (CIMP), and chromosome instability (CIN). The MSI pathway accounts for approximately 15% of CRC cases. In an inherited background named hereditary non-polyposis colorectal cancer (HNPCC), MSI results from germline mutations in DNA mismatch repair (MMR) genes such as *MLH1*, *MSH2*, *MSH6*, and *PSM2*. In sporadic cases, MSI most commonly results from epigenetic silencing of *MLH1* occurring in a background of methylation of CpG islands. (Rodriguez-Bigas et al., 1997; Sun et al., 2014). The CIMP pathway involves epigenetic instability and is characterized by vast CpG island promoter hypermethylation of a large number of genes, resulting in the inactivation of several tumor

suppressor genes or other tumor-related genes. CIN is the most prevalent type of genetic instability, occurring in 70 to 85% of tumors, encompassing insertions, inversions, deletions and rearrangements at the chromosomal level. The exact causal mechanism is not yet known. The many players involved play roles in mitotic checkpoints and other cell division mechanisms, including chromosome cohesion, centrosome copy number, kinetochore-microtubule attachment dynamics, and cell-cycle regulation. Defects in their function can lead to an increased occurrence of errors during chromosome segregation (Bolhaqueiro et al., 2019; Thompson et al., 2010). Loss of function of p53 protein is a significant event, as this protein is known as the "guardian of the genome", mainly responsible for inhibiting cell proliferation and promoting cell death in response to DNA damage. Therefore, when mutated, this gatekeeper function is lost, contributing to increased genomic instability and this loss is present in almost 50% of CRCs (Vousden & Prives, 2009). Analyses have indicated that mutations in other specific oncogenes or tumor suppressor genes such as *SMAD4* and *PIK3CA* are significantly more represented in CIN+ tumors.

It is known that the CIN pathway further increases the occurrence of oncogenic events and contributes to the appearance of a heterogeneous population of cancer cells with different properties and mutational profiles. This intratumoral heterogeneity (ITH) ultimately leads to treatment failure and is associated with poor clinical outcomes. A possible approach to target ITH is to functionally characterize the role of molecules defining the stem cell identity of a population of cancer cells as a way to tackle cellular heterogeneity (Hoevenaar et al., 2020).

1.2.2. Stem cells as cells of origin of CRC

The CRC microenvironment is characterized by a heterogeneous population of cells possessing different tumorigenic potentials and expressing different cell markers. In recent years, several studies have shown that CRC could originate from a population of cancer cells with stemness properties, many times named cancer stem cells (CSCs) or tumor-initiating cells (S. Srivastava et al., 2011). The subpopulation of CSCs has been characterized by their self-renewal capacity, proliferation, multidirectional differentiation, and mechanisms of therapy resistance. Therefore, new studies suggest that CSCs have a primary role in metastasis and treatment failure (Zheng et al., 2022).

Studies are being conducted to characterize and provide insights about CSCs. In a recent study, the CRC tumorigenic cell population was isolated, and the expression of specific cell

surface markers was observed, including LGR5. In mice, LGR5 expression was associated with adenomas' development, and the LGR5+ cell population has been suggested to be the cell of origin of malignant intestinal lesions (Barker et al., 2009). Similarly, in human CRC cases, the expression of a "stem cell signature," including the expression of LGR5 and ASCL2 stem cell markers has been observed (Ziskin et al., 2013). The LGR5 was also reported to be overexpressed and retain a prominent role in the proliferation of tumors, in the capacity of invasive distant metastatic tumors, and in poor clinical prognostics (Gao et al., 2014; Kleist et al., 2011; Liu et al., 2014). Because of that, there are efforts to understand the potential behind the LGR5+ cell populations as a possible therapeutic target since it has been reported to be preserved in some human CRC tissues (Shimokawa et al., 2017). Nonetheless, there are many conflicts about this topic and other markers have been studied in this context, and more in depth studies are necessary to fully sustain the concept of CSCs.

1.2.3. CRC mouse models

Mice models have been extensively used to study several human diseases since they are phylogenetically closer, presenting 90% of the genomic regions related to humans (Bürtin et al., 2020). In order to fully understand the impact of the molecular alterations that contribute towards CRC development it is necessary to establish and study experimental models that can adequately address the carcinogenic cascade. In that sense, different animal models of CRC have been developed over the last years. Many of the CRC mouse models are focused on the loss of the *Apc* gene, a common first step in colorectal carcinogenesis, together with activating mutations of *Kras*, as a way to mimic the progression from pedunculated adenomatous polyps to adenocarcinomas. Most of these models are conditional and established using the Cre/*loxP* gene targeting system. Cre is a site-specific recombinase that recognizes *loxP* sequences, causing the excision of DNA flanked by two *loxP* sites. Through the Cre/l*oxP* system, it is possible to activate or inactive genes in specific organs of interest using a Cre expressing strain for conditional recombination (Sauer, 1998). In this work, the *Fabpl*$^{+/Cre}$ expressing strain was used to direct Cre recombinase-mediated action specifically to the distal small intestine and colonic epithelia.

In most mouse models of CRC, loss of one *Apc* allele is sufficient to induce adenomas in the intestine, being that the *Apc* homozygous knockout (KO) is embryonically lethal. As such, conditional *Apc* mutant models were established using the *Apc*^{2Lox14} strain, in which

Cre recombination promotes the deletion of exon 14 and creates a frameshift mutation at codon A580, leading to *Apc* inactivation and intestinal adenoma development (Colnot et al., 2004). The same genetic system was used with *Kras*$^{LSL\text{-}G12D}$ strain to introduce an activating mutation in the oncogenic *Kras*, leading to widespread hyperplasia throughout the colonic epithelium (Haigis et al., 2008). Mutational activation of *Kras* alone is insufficient to initiate cancer in the mouse colon, but when combined with *Apc* inactivation it promotes the progression of adenomatous lesions to adenocarcinomas, hence combining these two genetically engineered models creates a new mouse model that better mimics human CRC cases. Nevertheless, most genetically engineered mouse models of CRC do not fully recapitulate the intrinsic ITH of human tumors, requiring additional mutations, for instance in *TP53*, to induce CIN.

1.2.4. CRC-derived organoids – tumoroid cultures

In the past years, the discussion about replacing animal models has been increasing, mainly due to ethical concerns. From this perspective, the scientific community is making considerable efforts towards this aim, creating alternative models. The discovery of LGR5 as a bona-fide marker of ISCs and a Wnt pathway member and target was a landmark in the stem cell field. This led to the discovery of the minimal growth factor cocktail and extracellular matrix (ECM) necessary for sustaining murine ISCs *ex vivo* in the form of 3D structures called intestinal organoids comprising all intestinal cell types (Sato et al., 2009). These structures can be established from intestinal crypts or even a single LGR5+ ISC. Furthermore, these cell cultures can grow as 3D structures using different scaffold systems, from the most commonly used matrigel to synthetic systems (Bédard et al., 2020).

The organoids 3D culturing system offers a vast possibility of studies such as mimicking the organ development process and regeneration, studying stem cells identity, drug testing, and cancer research (Cacciamali et al., 2022; Drost & Clevers, 2018). Nowadays, organoids are established from different tissue sources, including human cancer tissue, leading to the culture of primary colon cancer cells in the form of tumoroids to better recapitulate human disease (Van De Wetering et al., 2015). The scarce amount of clinical material available usually limits downstream applications. CRC tumoroid culture allows long-term expansion of tumor tissue with a high success rate (77-85%; (Yao et al., 2020), not easily achieved by other methods, and partially captures the heterogeneity of matched primary tumors. Hence, CRC tumoroid culture considerably reduces the number of animals used for research, while

at the same time allows the use of human derived material, contributing to increase physiological relevance.

1.3. CRISPR/Cas9 technology in tumoroids

Another key advantage of the use of tumoroid models is the possibility of streamlining gene manipulation with living culture systems. The revolutionary technology called Clustered Regularly Interspaced Short Palindromic Repeats (CRISPR) was first described in 1987 in *Escherichia coli* when the presence of repeating sequences of 29 nucleotides separated by unique sections of DNA was observed (Ishino et al., 1987). After that, the same regularly spaced repeated sequences were described in archaea, specifically in *Haloferax mediterranei* (F.J.M. Mojica et al., 1993). CRISPR-Cas is part of the bacteria and archaea defense system against infections by phages or the transformation by plasmids, as it allows modifications in genomic DNA at specific targets in different organisms and cell types, including insertions, deletions, and inactivation of target genes (Barrangou et al., 2007; Knott & Doudna, 2018; Makarova et al., 2006). The most widely employed CRISPR-Cas system employs the effector enzyme Cas9 from *Streptococcus pyogenes* to promote genome editing.

The Cas9 protein consists of two parts: the recognition (REC) and the nuclease (NUC) part (Figure 5). The REC part is responsible for recognition and complexes with the foreign DNA containing an adjacent protospacer motif (PAM). Meanwhile, the NUC contains two unrelated essential nuclease domains, the HNH and RuvC, essential for the Cas9 cleavage function, and a C-terminal region containing a PAM-interacting (PI) domain. Moreover, the correct targeting depends strictly on the presence of this PAM motif. The Cas9 protein acts by introducing double-stranded DNA breaks (DSBs) in a specific target genomic locus by DNA cleavage and then the target sequence passes through the major pathways for DNA damage repair (Yoshizumi et al., 2018). CRISPR-Cas9 system is a powerful tool already used in 3D cell culturing. The system permits the creation of specific mutations by designing sgRNAs to target genes. The capacity to model the colorectal carcinogenesis process by introducing multiple mutations by CRISPR-Cas9 technology was already established by targeting the *APC, SMAD4,* and *TP53* in human intestinal organoids, permitting them to evaluate the effect of each mutation in the CRC process (Matano et al., 2015). Because of that, CRISPR-Cas9 is one of the best technology options to help model the CRC disease since it is possible to study the role of each mutation individually, as KO or as overexpression.

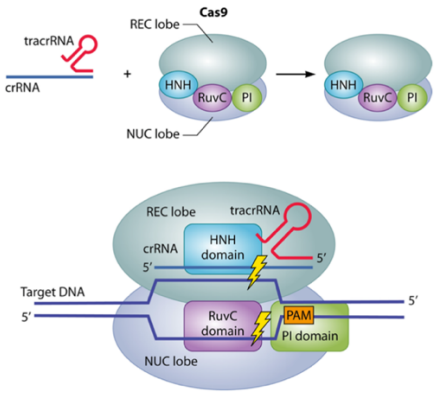

Figure 5 | The Cas9 protein. A schematic representation of the Cas9 protein complex, consisting in two distinct lobes: the recognition (REC) and the nuclease (NUC) lobe. The NUC lobe contains the PAM-interacting (PI) domain, the HNH and RuvC nuclease domains, responsible for cleaving the DNA strands. Adapted from Yoshizumi Ishino et al. (2018).

1.4. RNA-binding proteins

RNA-binding proteins (RBPs) are highly conserved proteins that can assemble RNA, playing a crucial function in all post-transcriptional events essential to maintaining homeostasis of gene expression in eukaryotic cells (Matia-González *et al.*, 2015). Because of that, RBPs together with non-coding (nc)RNAs regulate critical steps in the RNA life cycle (Figure 6), which include transcription, splicing, polyadenylation, transportation, localization, degradation, and translation (Dreyfuss *et al.*, 2002).

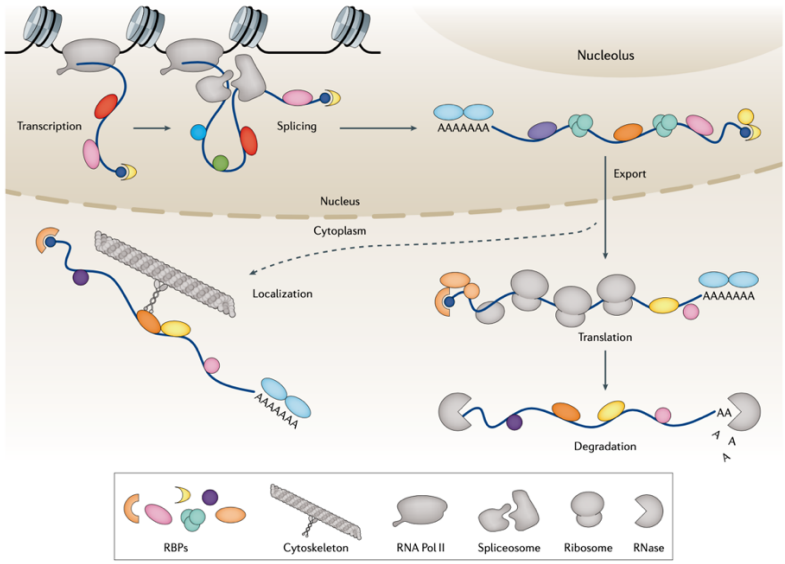

Figure 6 | RNA-binding proteins regulating RNA life cycle. A schematic overview of the post-transcriptional events in which RBPs participate. The illustration shows RBPs as ribonucleoprotein particles (RNPs) represented by the colored structures (RBP) assembled in the RNA (gray). Adapted from: Gebauer et al.(2021).

RBPs can bind in one or multiple RNA sites through RNA-binding domains (RBDs; Figure 7). When assembled, they form ribonucleoprotein complexes (RNPs), which are dynamic structures that can be easily reversed and are responsible for changing the fate or function of the bound RNAs involved (Dreyfuss et al., 2002). RBPs are extensively studied nowadays, and several studies show that they are highly preserved in bacteria, archaea, and eukaryotic cells. In this perspective, a group recently validated a set of 1,542 human RBPs by computational analyses, representing approximately 7,5% of all protein-coding genes (Gerstberger et al., 2014).

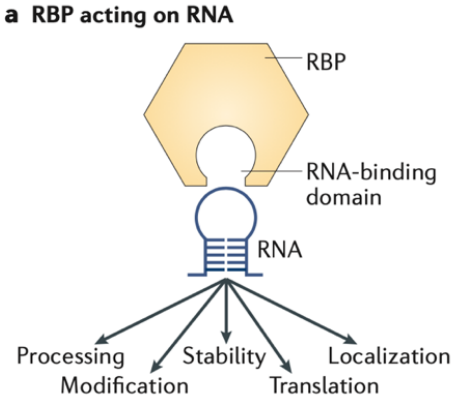

Figure 7 | RNA-binding protein acting on RNA. A representative image of the crosstalk between RBP and RNA and the possible RNA fate after being bound. Adapted from Hentze et al.(2018).

RBPs are usually classified based on their specific RBDs and their affinity to bind and interact with specific RNA sequences (Glisovic et al., 2008). The most common and well-characterized RBDs are the RNA recognition motif (RRM), K-homology (KH) domain, double-stranded RBD (dsRBD), and zinc-fingers domains (ZnF) (Burd & Dreyfuss, 1994).

Considering the importance of RBPs in post-transcriptional events, it now becomes evident that dysregulation of some RBPs can lead to several human pathologies, such as cancer (Gebauer et al., 2021). Several RBP families are dysregulated in different cancers, impacting the function and expression of tumor suppressor proteins and oncoproteins. The molecular mechanisms behind the role of RBPs in the initiation and progression of cancers are mainly associated with the capacity to sustain proliferation, evading apoptosis, and promote cell migration and invasion (Pereira et al., 2017).

Even though our understanding of the roles of RBPs in post-transcriptional mechanisms increased recently, there is a lot to be discovered. The function of RBPs on cancer is an

emerging research area with potential for the discovery of new therapeutic targets and biomarkers to predict cancer progression.

1.4.1. MEX-3 family of RNA-binding proteins

The RBP MEX-3 is a translational repressor firstly described in the nematode *Caenorhabditis elegans* by its role in controlling the localization of the caudal-like homeodomain protein PAL-1, which is an essential transcriptional activator during the development of the embryonic body wall muscle in the *C. elegans* embryo (Hunter & Kenyon, 1996). Dysfunctions in the *mex-3* gene produced an abnormal expression of PAL-1 in the anterior blastomere, developing an excess of body wall muscles in the anterior blastomere, hence the name *mex* for muscle excess (Draper et al., 1996; Hunter & Kenyon, 1996). In contrast, in adult worms, MEX-3 was reported to regulate germline stem cell totipotency (Ciosk et al., 2006).

The MEX-3 family encodes four homologous genes in humans and mice: *MEX3A*, *MEX3B*, *MEX3C,* and *MEX3D.* MEX3 proteins have two highly conserved RNA-binding KH domains, responsible for recognizing a MEX-3 recognition element (MRE) in the 3'-UTR of target RNAs defined as the degenerate consensus sequence (A/G/U)(G/U)AGN$_{(0-8)}$U(U/A/C)UA (Pagano et al., 2009). In addition, besides these KH domains, there is a Really Interesting New Gene (RING) finger domain at the C-terminal tail with putative E3 ubiquitin ligase activity (Cano et al., 2010).

Thus far, it is known that MEX-3 family members are involved in post-transcriptional regulatory mechanisms associated with different cellular processes. From this perspective, MEX3B was correlated with innate immune responses and fertility in mice (Le Borgne et al., 2014; Yang et al., 2016). MEX3C was related with the decay of HLA-A allotypes (Cano et al., 2012) and regulation of energy balance (Jiao et al., 2012). MEX3D is the least studied member showing a ubiquitous expression pattern (Buchet-Poyau et al., 2007). Nonetheless, like other RBPs, the MEX-3 family members play roles in both homeostasis and disease. It has been described a differential expression of MEX-3 proteins in different cancer types relative to normal tissues, suggesting that some of their targets are cancer-relevant proteins (Huang et al., 2018; Pereira et al., 2017).

1.4.2. MEX3A protein

Concerning *MEX3A*, it is localized in chromosome 1q22 in humans and codifies a nuclear and cytoplasmatic protein with a molecular weight of around 65kDa. The *Mex3a* transcript was reported as part of the *Lgr5*+ stem cell signature in the mouse intestine (Muñoz et al., 2012). Besides, MEX3A was also detected in a small group of murine LGR5+ ISCs resistant to chemotherapy and radiation (Barriga et al., 2017). In line with these observations, our group established and characterized the first *Mex3a* KO mouse model. The results showed that the KO mice were smaller in size, with higher mortality rates pre and postnatal than heterozygous and wild-type strains (Figure 8A). Importantly, we found that MEX3A is expressed in mouse ISCs and is responsible for maintaining the LGR5+ ISCs and subsequent intestinal turnover, as showed by the loss of *Lgr5*+ cells in the intestinal crypts of the KO mice (Figure 8B). These alterations are possibly associated with a change in the cellular differentiation and metabolic profiles mediated by the Peroxisome Proliferator-Activated Receptor (PPAR)γ signaling pathway (Pereira et al., 2020). PPARγ is a nuclear receptor isotype that, when activated, leads to the transactivation of target genes involved in metabolic homeostasis and cellular differentiation (Dubois et al., 2017). We observed that MEX3A overexpression in Caco-2 colorectal cancer cells leads to a significant decrease in PPARγ protein levels, impairing activation of the pathway. Moreover, we observed an accentuated decrease in *Lgr5* mRNA expression levels specifically in *Mex3a* KO intestinal organoids upon exposure to a PPARγ agonist from the glitazone drug family, impairing new organoid formation upon passaging (Pereira et al., 2020). This was the first study to characterize the role of MEX3A as a specific functional ISC marker necessary for maintaining the LGR5+ ISCs population and to suggest the MEX3A impact on intestinal homeostasis, probably through regulation of the PPARγ signaling.

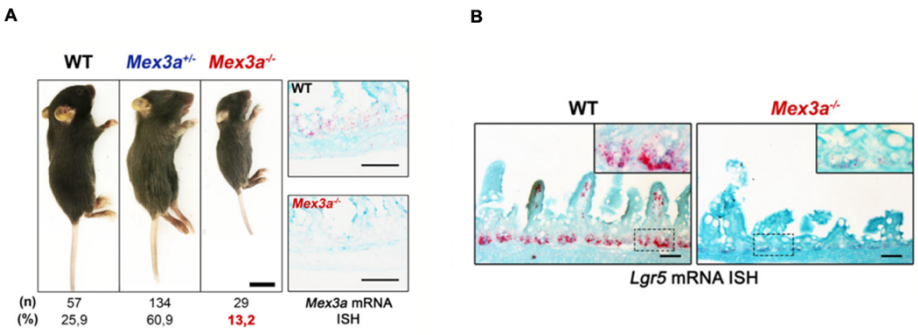

Figure 8 | The first *Mex3a* knockout mice. B) Representative images of the size of Mex3a mutant mice compared to the heterozygous and wild-type strains; H) ISH showing that Mex3a KO leads to loss of $Lgr5^{+}$ stem cells and damages for crypt development. Adapted from Pereira et al. (2020).

1.4.3. The role of MEX3A protein in different cancer types

In a cancer context, *MEX3A* has been shown to be overexpressed in several malignant models. Accordingly, many studies propose that this RBP could be a potential therapeutic target and work as a prognostic predictor in several cancer types.

Our group demonstrated that MEX3A is involved in the regulation of intestinal differentiation and cell cycle progression in gastrointestinal cancer cell lines, in addition to promoting an increase in the expression of specific ISC markers, such as *LGR5*, *BMI1* and MS1, through the downregulation of the intestinal transcription factor CDX2, promoting a loss of cellular differentiation (Pereira et al., 2013). Additionally, it was reported that inhibition of *MEX3A* expression affects proliferation and migration of gastric cancer cells (Jiang et al., 2012).

Recently, a group demonstrated that *MEX3A* is overexpressed and correlated with low levels of retinoic acid-inducible gene I (RIG-I) protein in glioblastoma multiforme (GB), the most aggressive primary brain tumor (Bufalieri et al., 2020). RIG-1 is a tumor suppressor essential to regulate differentiation and apoptosis. The group observed that MEX3A binds RIG-1, inducing ubiquitylation and proteasome-dependent degradation, thus describing a new molecular mechanism. These new findings were significant for GB biology because they suggest that MEX3A and RIG-1 might be promising therapeutic targets in a very lethal cancer type.

The role of MEX3A in lung cancers is also starting to be addressed. MEX3A is overexpressed in lung adenocarcinoma (LUAD) tissues and is associated with poor clinical outcomes. They also demonstrated by RNA-immunoprecipitation (RIP) assay that MEX3A binds the laminin subunit alpha 2 (*LAMA2*) mRNA, increasing proliferation in LUAD cells. Moreover, they suggest that MEX3A and LAMA2 could influence the PI3K-AKT signaling pathway, suggesting that both can serve as prognostic biomarkers for LUAD and as therapeutic targets (Liang et al., 2020).

The higher expression of *MEX3A* was already observed in triple-negative breast cancer (TNBC), associated with poor clinical prognosis and malignancy. Downregulation of MEX3A inhibits tumor growth, while overexpression stimulates cancer development. Additionally, an association between MEX3A and the PI3K-AKT signaling pathway was verified, as MEX3A overexpression and treatment with PI3K-AKT signaling pathway inhibitors lead to

a decrease in tumor growth (S. Jiang et al., 2020). These findings support the same results in LUAD cancer.

Finally, a higher expression of MEX3A was observed in pancreatic ductal adenocarcinoma (PDAC), one of the most aggressive and lethal cancers in the world. High levels of MEX3A proved to have prognostic value for the development of chemoresistance in PDAC patients (Panzeri et al., 2021).

Chapter 2 | Objectives

We recently demonstrated that MEX3A is specifically expressed in mouse ISCs and responsible for maintaining the LGR5+ ISC population by repressing the PPARγ differentiation pathway, thus contributing to intestinal homeostasis. Additionally, our group is studying the role of MEX3A in the process of colorectal carcinogenesis through the study and characterization of CRC mouse models and human CRC cases. However, the specific function of MEX3A in this cancer context is still not fully disclosed.

Our working hypothesis is that MEX3A-mediated stem cell identity might contribute to ITH in a context of CIN. To address this, the main objectives of this work were to establish and characterize CIN+ CRC-derived tumoroids with MEX3A modulation as physiologically relevant models to determine the functional impact of MEX3A on CRC progression. We have three specific aims:

1. To establish colorectal cancer-derived tumoroids to model CRC in early and late stages;

2. Modulate the expression of MEX3A in physiologically relevant models to determine the functional impact of MEX3A on CRC progression;

3. To characterize these models concerning the onset of CIN using quantification of chromosome segregation errors.

Chapter 3 | Material and methods

3.1. Animal models

Different mouse strains were used for this work. The *Apc*$^{+/\Delta ex14}$, *Kras*$^{+/G12D}$ and *Fabpl*$^{+/Cre}$ strains were all a kind gift from Sérgia Velho (Epithelial Interactions in Cancer group, i3S). The *Mex3a* KO strain was generated at the National Centre of Biotechnology (CNB-CSIC, Madrid, Spain). These were crossed to generate compound *Apc*$^{+/\Delta ex14}$;*Kras*$^{+/G12D}$;*Fabpl*$^{+/Cre}$;*Mex3a*$^{+/-}$ animals and the corresponding *Apc*$^{+/\Delta ex14}$;*Kras*$^{+/G12D}$;*Fabpl*$^{+/Cre}$ control mice. All mice were raised and maintained at the animal facility of i3S, which is accredited by the Association for Assessment and Accreditation of Laboratory Animal Care (AAALAC). The standard conditions were a 12-hour light/dark cycle, with water and rodent chow available all the time.

Animal experiments were carried out following the Portuguese National Regulation established by Decreto-Lei 113/2013 upon the national implementation of European Directive 2010/63/EU laws for the Care and Use of Laboratory Animals. All procedures were evaluated and approved by the i3S Animal Welfare and Ethics Review Body (ORBEA) and by the Portuguese National Authority for Animal Health (DGAV) - project license code 015434/2017-07-04. The researchers that performed procedures with animal models in this work are certified in animal experimentation (FELASA C course).

3.2. Human samples

Surplus fresh tumor tissue and adjacent non-tumor tissue were obtained from patients diagnosed with CRC and performing colonic surgeries at IPO-Porto under informed consent, in accordance with an established protocol approved by the IPO Ethics Committee and following the principles of the Declaration of Helsinki. Importantly, the collection of this supplementary biological material did not imply additional risks for the patient besides the ones associated with the surgical procedure already taking place. Personal and clinical information is managed by IPO that implements security clearance access and sample anonymity to safeguard patient identity. The human material used will be part of a larger experimental study, which is currently under review by the IPO Ethics Committee, through a kind collaboration with Professor Carmen Jerónimo (group Leader of the Cancer Biology & Epigenetics Group and the Scientific Coordinator of the Biobank at IPO).

3.3. Conditioned media production for organoid culture

Stably transfected HEK293T human cells were used for mouse R-spondin1 (RSPO1) and Noggin (NOG)-conditioned media (CM) production. The RSPO1-producing cell line was a kind gift from Calvin Kuo (Stanford University, USA) and NOG producing cell line was a kind gift from Gijs van den Brink (Tytgat Institute, University of Amsterdam, Netherlands). Commercially available murine L-cells stably transfected to express WNT3A (ATCC CRL2647) were used to produce WNT3A-CM.

All cell lines were cultured in DMEM (Thermo Fisher Scientific) with 10% (v/v) fetal bovine serum (FBS; Biowest), 1% (v/v) Penicillin-Streptomycin (Thermo Fisher Scientific) and appropriate selection antibiotics in T75 flasks and maintained in an incubator at 37ºC with 5% (v/v) CO_2. When cells reached confluence, they were split into 4 T75 flasks with complete DMEM, but without selection antibiotics. Upon reaching confluence, cells from 2 T75 were combined into a T175 culture flask with AdvancedDMEM/F12 (AdvDMEM/F12, Thermo Fisher Scientific), 10% (v/v) FBS, 1x GlutaMAX (Thermo Fisher Scientific), and 10 mM HEPES (Thermo Fisher Scientific). After 7 days in culture, the CMs were collected, centrifuged, filtered with a 0.22 µm PES filter and stored at -20ºC until further use.

3.4. Organoid culture establishment and maintenance

Colon organoid and tumoroid lines were established from both mouse models and human CRC patients based on previously published protocols (Sato, Stange, et al., 2011; Van De Wetering et al., 2015) with further optimization and considering the mutational profile of the corresponding primary tumors.

In the case of the mouse models, *Apc*$^{+/F}$;*Kras*$^{+/G12D}$;*Fabpl*$^{+/Cre}$;*Mex3a*$^{+/-}$ mice and littermate-matched *Apc*$^{+/F}$;*Kras*$^{+/G12D}$;*Fabpl*$^{+/Cre}$ animals were euthanized (usually around 9 weeks of age) upon presentation of signs of CRC onset. After euthanasia, the whole colon was flushed with ice-cold PBS to remove fecal contents and opened lengthwise. Tumor tissue foci were macroscopically separated from adjacent non-tumor tissue and cut into small pieces of around 5 mm^2. Then, the epithelial component was detached from the underlying mesenchymal compartment by incubation with a mixture of proteolytic and collagenolytic enzymes for 15 min at 37ºC with agitation. The undigested tissue fragments were allowed to settle down by gravity and tumor cell aggregates/single cells present in the supernatant were collected by centrifugation. These were embedded in Matrigel growth factor reduced basement membrane matrix (Amsbio), the cell/matrix suspension placed in each well of a

pre-warmed 24-well plate and incubated for 20 min at 37ºC, 5% CO_2. After Matrigel polymerization, 500 µL of mouse colon tumoroid medium composed of AdvDMEM/F12 supplemented with HEPES (10 mM), GlutaMAX (1X), B-27 (1X), N-2 (1X), 10% (v/v) NOG-CM, Primocin (100 µg/mL), and Y-27632 (10 µM) was added to each well. For the ligand stimulation experiments, tumoroids were treated for 5 consecutive days with 50 µM of the PPARγ-selective agonist Rosiglitazone (Tocris Bioscience) or with the same volume of the vehicle (DMSO).

In case of CRC patients, the initial tumor and (adjacent) non-tumor fragments were divided for histology, genetic analysis and culture. For the latter, the epithelial component was macroscopically separated from visible adipose/mesenchymal tissue and cut into small pieces below 5 mm^2. Epithelial enrichment was achieved by incubation with a mixture of proteolytic and collagenolytic enzymes for 30 min at 37ºC with strong mechanical agitation. Normal-like colon crypts and tumor cell aggregates/single cells were obtained from each type of tissue, embedded in Matrigel (Corning) and plated as indicated above. In addition to the components of the mouse colon tumoroid medium, the human colon organoid media was further supplemented with N-Acetylcysteine (1.25 mM), 10% (v/v) RSPO1-CM, 50% (v/v) WNT3A-CM, EGF (50 ng/mL; Peprotech), gastrin (10 nM; Merck), A 83-01 (500 nM; StemCell Technologies), and SB202190 (5 µM; StemCell Technologies). The human colon tumoroid media is the same as the human colon organoid media, although two different culture conditions have been employed: with and without WNT3A-CM.

The culture medium was replaced every two days, and cultures were enzymatically passaged every week (in case of mouse tumoroids) or every two weeks (in case of human organoids and tumoroids), expanded, used for different experimental settings and cryopreserved for long-term storage.

3.5. Genome editing by CRISPR-Cas9 technology

The plasmid pSpCas9(BB)-2A-GFP (PX458), established by Feng Zhang lab (Addgene plasmid #48138), was selected for this project based on its specific characteristics: expression of the widely used *Streptococcus pyogenes* Cas9, expression of a EGFP reporter and for having the cloning backbone for single-guide (sg)RNAs (all-in-one vector; Figure 9).

In this work, the PX458 vector was used for cloning sgRNAs to KO two different genes*:* *Trp53* in mouse colon tumoroids and *MEX3A* in human colon tumoroids. The mouse *Trp53* and human *MEX3A*-specific sgRNAs were designed using the UCSC Human Genome Browser software to identify guide sequences in regions of interest (Kent et al., 2002).The sgRNAs consist of a 20-nt guide sequence preceded by a 5′-NGG adjacent motif (PAM). The guides were selected considering a MIT Guide Specificity score > 60 (the higher the percentage, the fewer off-target effects) and a Doench 2016 Efficiency score > 70 (the higher the percentage, the stronger the cutting efficiency). The *MEX3A* sgRNA (sgRNA MEX3A#3) PX458 construct used was already assembled and previously tested, a kind gift by Ana Rita Silva, PhD student (Differentiation and Cancer group, i3S). The sgRNAs sequences and scores are provided in Table 1.

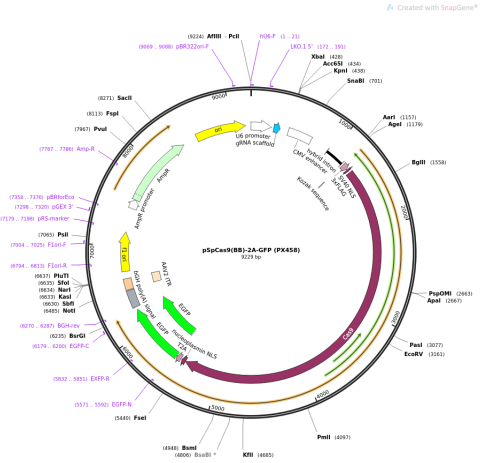

Figure 9 |The pSpCas9(BB)-2A-GFP (PX458) plasmid map.

Table 1 | Designed guides sequences for *Trp53* KO and MEX3A KO and their scores.

NAME	PRIMER	GUIDE SEQUENCE (5´-3´)	MIT Specificity score	Efficiency score (%)*
sgRNA p53 #3 (-)	sgRNA - top	CACCGAACAGATCGTCCATGCAGTG	72	98
	sgRNA - bottom	AAACCACTGCATGGACGATCTGTTC		
sgRNA p53#4 (-)	sgRNA - top	CACCGAGGAGCTCCTGACACTCGGA	86	72
	sgRNA - bottom	AAACTCCGAGTGTCAGGAGCTCCTC		
sgRNA p53#5 (+)	sgRNA - top	CACCGAAGTCACAGCACATGACGG	84	97
	sgRNA - bottom	AAACCCGTCATGTGCTGTGACTTC		
sgRNA Mex3A#3 (+)	sgRNA - top	CACCGCCTACATCAAGACACCGGTG	93	99
	sgRNA - bottom	AAACCACCGGTGTCTTGATGTAGGC		

To assemble the CRISPR-Cas9 expression system, a previously published protocol from Ran et al. was followed as described below (Ran et al., 2013). Briefly, the designed sgRNAs were first processed for insertion in a plasmid by incubation in a thermocycler with a mixture for phosphorylation and annealing of both sgRNA strands. Next, the sgRNA oligos were cloned into the pSpCas9(BB)-2A-GFP vector by an incubation step for 1 h in a thermocycler using a FastDigest BbsI restriction enzyme and a T4 ligase mixture. The plasmids were used to transform chemically competent StbI3 Escherichia coli strain according to the manufacturer's protocol. After the transformation step, plasmid DNA was isolated using NZYMiniprep (NZYTech) according to the manufacturer's guidelines. DNA concentration was quantified using a NanoDrop ND-1000 spectrophotometer (Thermo Fisher). Sanger sequencing was performed to confirm the correct insertion into PX458 using the BigDye Terminator v3.1 Cycle Sequencing kit (Thermo Fisher Scientific). Briefly, a mixture composed of the plasmid DNA (150-300 ng), U6 promoter sequencing primer (10 µm) and the Big Dye Sequencing RR100 solution was prepared in PCR tubes. The sequencing PCR conditions were 1 min at 96ºC (1x), 10 s at 96ºC, 5 s at 50ºC (25x), 4 min at 60ºC, and a holding step at 4ºC (1x). Before analysis, the sequencing products were purified using Sephadex G-50 Fine DNA Grade columns (GE Healthcare).

3.6. Tumoroid transfection

3.6.1. Tumoroid transfection for *Trp53* KO in mouse tumoroids

Transient transfection of mouse-derived colon tumoroids for *Trp53* KO was performed using Lipofectamine 3000 (Thermo Fisher), according to the manufacturer's instructions. First, the tumoroids were dissociated as previously described, and the cells were counted. For transfection, 1.5 x 10^5 cells were used from *Apc*$^{+/F}$;*Kras*$^{+/G12D}$;*Fabpl*$^{+/Cre}$;*Mex3a*$^{+/-}$ and *Apc*$^{+/F}$;*Kras*$^{+/G12D}$;*Fabpl*$^{+/Cre}$ tumoroids. Then, sgRNAs were diluted in OPTI-MEM (Thermo Fisher Scientific) and added to a mix composed of Lipofectamine 3000, Y-27632 and Polybrene (10 µg/mL; Thermo Fisher) also diluted in OPTI-MEM. The cells were centrifuged and incubated for transfection. Afterward, the transfected cells were plated in a 24-well plate and seeded with 500 µL of tumoroid medium as previously described. After 48 h, the tumoroids were analyzed in a ZOE Fluorescent Cell Imager (Bio-rad) to verify the expression of the GFP reporter and estimate transfection efficiency. For selection of p53 KO tumoroids, 72 h after transfection the tumoroids were treated with 5 µM Nutlin-3a (Merck) for 5 days. After 2 weeks of selection, the tumoroids were dissociated and seeded for clonal expansion.

3.6.2 Tumoroid transfection for *MEX3A* KO in human tumoroids

The transfected protocol for MEX3A KO used a human colon tumoroid line (005T Wnt) to create the KO tumoroids. The transfection was performed using Lipofectamine 2000 (Thermo Fisher), according to the manufacturer's instructions. In this instance, the transfection was performed using 1,5 x 10^5 cells plated in a collagen type I (ibidi) layer one day before. After 48 h of transfection, the GFP reporter expression was analyzed to confirm transfection efficiency. After 4 days, fluorescence-activated cell sorting (FACS) was performed to isolate the single cells expressing the GFP reporter using the BD FACSAria sorter (BD Biosciences) in i3S Translational Cytometry unit. For FACS, the cells were enzymatically collected, resuspended in FACS buffer, and filtered through a FACS tube. After sorting for GFP expression, single cells were plated in a collagen-coated 96-well plate. The *MEX3A* KO clones were grown in collagen for several weeks (depending on clone fitness). When the clones reached the necessary confluence, they were transferred to Matrigel culture and subsequently expanded.

3.7. Organoid live cell imaging

Live-cell imaging of colon organoids was performed using a confocal laser-scanning microscope (Leica SP5). Five days before the imaging session, the cells were dissociated as previously indicated. Then, 10 µL of the single cell/Matrigel suspension was plated in a µ-Slide 8 Well (Ibidi) and covered with 300 µL of the corresponding culture media. On the day of recording, the culture medium was changed by fresh medium containing SPY505-DNA and SPY555-tubulin, non-toxic and cell-permeable probes for fluorescence live imaging of DNA and microtubules, respectively.

Organoid images were captured in xyzt mode for at least 3 h, at 37ºC and 5% CO_2 conditions, with 2,5-3 min intervals using a 40x water-immersion objective. Around 10 z-sections at 0,5-1 µm intervals were imaged per organoid at a 400 Hz speed. The image analysis was performed using ImageJ/Fiji software. Organoids were classified according to different categories of segregation errors: Anaphase bridge, Lagging chromosome, Multipolar, and no error.

3.8. Protein extraction and quantification

Protein extraction was performed by using RIPA lysis buffer [20 mM Tris-HCl (pH 7.5), 150 mM NaCl, 2 mM EDTA (pH 7.5), 1% (v/v) Nonidet P-40, 0,1% (v/v) sodium dodecyl sulfate

(SDS), 0,5% (v/v) sodium deoxycholate] supplemented with 1 mM phenylmethylsulfonyl fluoride (PMSF), 20 mM sodium fluoride (NaF) and 1 mM sodium orthovanadate (Na_3VO_4) [all three from Merck] and 1 x Complete protease inhibitor cocktail (Roche Applied Science). Cells were lysed on ice for 30 min, resuspending the mix every 10 min. Next, the lysates were centrifuged for 15 min at 16000 xg at 4ºC, and the supernatant was collected.

Protein quantification was done using the Pierce BCA Protein Assay kit (Thermo Fisher Scientific), following the manufacturer's instructions. Briefly, 5 µL of each sample to be quantified (diluted 10x) was placed in duplicate in a 96-multiwell plate, along with 5 µL of bovine serum albumin (BSA) solutions of known concentration. A solution consisting of 195 µL of reagent A + B (50:1) was added to each well and the plate incubated for 30 min at 37ºC. Absorbance was read at 562 nm on a Synergy Mx multi-mode microplate reader (Biotek). The results were used to create the standard curves and calculate each sample's protein concentration.

3.9. Western blot analysis

To prepare the protein samples for SDS PolyAcrylamide Gel Electrophoresis (SDS-PAGE), a mix composed of 20 µg of extracted protein, 4 µL of loading buffer [4x Laemmli solution, 5% (v/v) β-mercaptoethanol (Sigma-Aldrich), and 5% (v/v) bromophenol blue solution (Sigma-Aldrich)] and dH_2O to complete 16 µL total volume was prepared in Eppendorf tubes. The samples were denatured for 5 min at 95°C and then loaded into a previously prepared 1 mm thick SDS-PAGE gel together with a Precision Plus Protein Dual Color Standards (Bio-Rad) molecular marker to estimate protein size. The gel ran at 140 V for 90 min in 1X Tris-Glycine-SDS Buffer (Bio-Rad). Proteins were then transferred to a nitrocellulose membrane (GE Healthcare Life Sciences) using 1x Tris-Glycine Buffer (Bio-Rad) with 20% (v/v) methanol (Thermo Fisher Scientific) on ice at 60 V for 2 h. Next, Ponceau Red (Sigma-Aldrich) staining was used to check for correct protein transfer.

For Western blot analysis, the protein membrane was first incubated with 5% (w/v) BSA (Sigma-Aldrich) in TBST [TBS (Grisp), 0,1% (v/v) Tween (Sigma- Aldrich)] for 1 h at room temperature (RT) with agitation to block unspecific antibody binding. The primary antibodies were prepared according to the supplier`s instructions and incubated overnight (ON) at 4°C with gentle agitation. On the following day, primary antibody excess was removed with 3 washing steps of 10 min each with TBST under agitation. Next, the membrane was incubated with the appropriate secondary antibodies diluted in 5% (w/v) milk for 1 h at RT

with agitation, followed by washing steps as previously described. To detect the proteins of interest, the membrane was incubated with the ECL Western Blot Detection Reagent (GE Healthcare Life Sciences) for 5 min at RT. The membrane was placed in a Hypercassette (Amersham Biosciences), and the Amersham Hyperfilm ECL (GE Healthcare) was used inside a dark room to detect the protein signals with variable exposure times by manually incubating the film with a developer and fixative solutions (Fujifilm). Actin levels were used to normalize protein expression, and quantification was performed using Fiji software.

The primary and secondary antibodies used for Western blot as well as their working concentrations are listed in Appendix A.

3.10. RNA extraction and quantitative real-time PCR

Total RNA was extracted using TRI Reagent (Merck) according to the manufacturer's guidelines. Briefly, 500 µL of TRI reagent was used to lyse cells by pipetting up and down, lysates incubated for 5 min at RT, 100 µL of chloroform (Sigma-Aldrich) added and samples vigorously vortexed for 15 sec, followed by an incubation period of 15 min at RT and centrifugation at 12000 xg for 15 min at 4ºC. After this step, the upper aqueous phase containing the RNA was carefully retrieved to a clean tube, mixed with 250 µL isopropanol, pulse-vortexed, followed by an incubation period of 10 min at RT and centrifugation at 12000 xg for 10 min at 4ºC. The pellet was washed twice with ice-cold 70% ethanol, left to dry for 10 min and eluted in dH_2O. RNA was quantified using a NanoDrop ND-1000 spectrophotometer and 2 µg of total RNA reverse-transcribed using a Reverse Transcriptase kit following the supplier guidelines (NZYTech).

Analysis of mRNA expression was performed by quantitative real-time PCR in an ABI Prism 7500 system using the Power SYBRGreen PCR Master Mix (Life Technologies) and sequence specific primer pairs spanning exon-exon junctions. Each sample was amplified in technical triplicates, and dissociation analysis confirmed the specificity of reactions. Gene expression was calculated using the relative quantification standard curve method, with *18S* rRNA levels measured to normalize target gene abundance. The primer pairs used for real-time quantification are listed in Appendix A.

3.11. Histochemical procedures

Human tissue samples and organoid cultures were formalin-fixed for a minimum of 48 h and paraffin processed following either a standard protocol or a Histogel (Thermo Fisher

Scientific) embedding step in case of the latter. For all histological procedures, slides were first deparaffinized and rehydrated, following standard steps. Briefly, deparaffination of the slides was achieved with two xylene solutions (Thermo Fisher Scientific) for 10 min each. Then the slides were re-hydrated through a series of ethanol solutions at 100% (v/v), 100% (v/v) and 70% (v/v) for 5 min each. To complete the rehydration, the slides were washed for 5 min in running tap water.

For morphological analysis, Hematoxylin and Eosin (H&E) staining was performed using 3 μm thick sections. The slides were stained in Modified Mayer's Hematoxylin (Thermo Scientific) for 5 min, followed by washing for 2 min in tap water, then immersed in 1% (v/v) ammonia water (Merck) for 2-3 sec and washed in tap water for 2 min again. The counterstain was performed in Eosin solution (Thermo Fisher Scientific) for 3 min followed by differentiation with 95% (v/v) ethanol for 3 min.

To assess cellular differentiation, the Alcian Blue-Periodic acid-Schiff (AB-PAS) reaction was performed using 3 μm thick sections. The tissues were stained with 1% Alcian Blue pH 2.5 (Merck) for 45 min and then treated with 0,5% Periodic acid (Thermo Fisher Scientific) for 10 min and stained with Schiff's reagent (Thermo Fisher Scientific) for 15 min. After each staining, the slides were washed with distilled water. To counterstain the nuclei, Modified Mayer's Hematoxylin was used for 5 min, and slides washed in running tap water for 5 min.

After each type of staining, dehydration was done through a series of one 95% (v/v) ethanol and two 100% ethanol solutions for 3 min each. Finally, the slides were clarified in two xylene solutions for 5 min each. The slides were mounted with Bio Mount HM (Bio-Optica) and air dried for at least 1 h.

3.12. Immunohistochemistry (IHC)

The immunohistochemistry technique was performed using 3 μm thick slides. After deparaffination and hydration, slides were placed inside Coplin jars with 10 mM citrate buffer pH 6.0 or 10 mM Tris-EDTA pH 8.0 solutions (depending on the antigen; both from Thermo Fisher Scientific) and subjected to heat-induced antigen retrieval in a steamer (Black & Decker) at 99°C for 40 min. Next, the slides were cooled for 20 min at RT and washed two times with TBST [0,05% (v/v) Tween] for 2 min each. All sections were delineated by a hydrophobic IHC Dako Pen (Dako). Endogenous peroxidase activity was blocked with an aqueous solution of 3% (v/v) hydrogen peroxide (Merck) for 10 min at RT,

and then the slides were rewashed as previously described. Afterward, the slides were incubated with primary antibodies, according to supplier indications, diluted in antibody diluent OP Quanto (Epredia) overnight at 4ºC.

On the next day, the slides were washed two times with TBST for 5 min and then incubated with a Rabbit/Mouse secondary antibody peroxidase-conjugated polymer system named REAL EnVision Detection System, Peroxidase/DAB (Dako) for 30 min at RT. After two more washing steps, slides were incubated with Diaminobenzidine (DAB; Dako) diluted in a solution of Dako REAL Substrate Buffer for 5min at RT. Finally, the slides were washed in running tap water for 5 min, counterstained in Hematoxylin, dehydrated and mounted as previously described.

The full list of antibodies used for immunohistochemistry as well as their optimized concentrations are listed in Appendix A.

3.13. mRNA *in situ* hybridization (ISH)

All the mRNA *in situ* hybridizations were executed following the protocol from RNAscope 2.5 HD Detection Reagent RED guide (Advanced Cell Diagnostics). The hybridizations were performed in 5 µm thick tissue sections. First, the slides were baked for 1 h at 60ºC, deparaffinized twice in xylene for 5 min each, and twice in 100% ethanol for 1 min. Next, the slides were incubated with RNAscope Hydrogen Peroxide for 10 min at RT and washed twice in dH_2o for 2 min. Then, they were subjected to the Standard pretreatment conditions, including i) a heat-induced target retrieval step using the RNAscope Target Retrieval solution for 15 min on a steamer, after which the cell/tissue sections were encircled by an IHC Dako Pen to create a hydrophobic barrier and left air-drying ON, and ii) an enzymatic treatment using the RNAscope Protease Plus solution for 15 min in a HybEZ hybridization oven (Advanced Cell Diagnostics) at 40ºC, followed by wash steps in dH_2O.

Probes against *MEX3A* and *LGR5* mRNAs (both from Advanced Cell Diagnostics) were used to perform the first hybridization step for 2 h at 40ºC. Next, the slides were passed by a series of hybridization steps at 40ºC: AMP1 for 30 min, AMP2 for 15 min, AMP3 for 30 min, and AMP4 for 15 min. The two final hybridization steps were performed at RT: AMP5 for 40 min (LGR5) or 1 h (MEX3A), and AMP6 for 15 min. Between all hybridization steps, the slides were washed two times for 2 min with agitation using the 1X Wash buffer. For signal detection, the Fast-Red chromogen was used for 10 min at RT, followed by a wash

step in dH_2O. Counterstaining was done using the Fast Green stain solution (Thermo Fisher Scientific) for 1 min. Finally, the slides were baked for 15min at 60ºC to let them dry and mounted with Vectamount (Vector Laboratories).

The mRNA probes used and their references are provided in Appendix A.

3.14. Statistical analysis

Each experiment was carried out at least three times. Statistical analysis was performed using GraphPad Prism, and the results are expressed as a percentage or mean ± standard deviation (SD). The Student's *t*-test was used to compare the means between different conditions. Differences between groups were considered statistically significant at a *P* value < 0.05.

Chapter 4 | Results

4.1. Establishment of *Apc*$^{+/F}$;*Kras*$^{+/G12D}$;*Fabpl*$^{+/Cre}$;*Mex3a*$^{+/-}$ mouse-derived CRC tumoroids

To start addressing the impact of MEX3A on CRC, we established a mouse model with altered (decreased) MEX3A expression, the *Apc*$^{+/F}$;*Kras*$^{+/G12D}$;*Fabpl*$^{+/Cre}$;*Mex3a*$^{+/-}$ strain, which was derived from the *Apc*$^{+/F}$;*Kras*$^{+/G12D}$;*Fabpl*$^{+/Cre}$ mouse that is a model for early stage CRC.

Independent cohorts of age-matched *Apc*$^{+/F}$;*Kras*$^{+/G12D}$;*Fabpl*$^{+/Cre}$;*Mex3a*$^{+/-}$ and *Apc*$^{+/F}$;*Kras*$^{+/G12D}$;*Fabpl*$^{+/Cre}$ animals (n = 3, each) were obtained and monitored for signs of disease starting at 7 weeks of age, mainly consisting of rectal prolapse development, rectal bleeding and low body condition score. Upon clinical presentation of any of these signs by one of the animals in the cage, the cohort was sacrificed. Macroscopic examination consistently revealed a decreased tumor area in the distal colon of *Apc*$^{+/F}$;*Kras*$^{+/G12D}$;*Fabpl*$^{+/Cre}$;*Mex3a*$^{+/-}$ mice when compared to *Apc*$^{+/F}$;*Kras*$^{+/G12D}$;*Fabpl*$^{+/Cre}$ animals (Figure 10). No macroscopic lesions were ever observed in the small intestine.

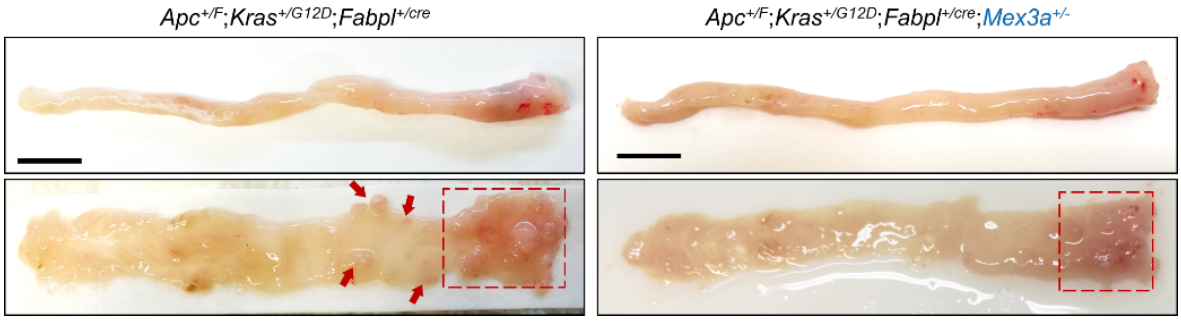

Figure 10 |Typical CRC lesions present in the colon of *Apc*$^{+/F}$;*Kras*$^{+/G12D}$;*Fabpl*$^{+/Cre}$ and *Apc*$^{+/F}$;*Kras*$^{+/G12D}$;*Fabpl*$^{+/Cre}$;*Mex3a*$^{+/-}$ mice. The upper panels show the dissected large intestine from the indicated mouse strains. The lower panels show the same gut tube opened. Tumor burden is depicted in the most distal part of the colon (red squares). Scale bars: 1 cm.

To obtain evidence concerning a specific role for MEX3A in affecting cancer cells behavior, we processed the tumor tissues from the previously mentioned animal models to establish epithelial tumoroid cultures. After culture stabilization, differences in tumoroids size and morphology were clearly observed. Overall, *Apc*$^{+/F}$;*Kras*$^{+/G12D}$;*Fabpl*$^{+/Cre}$;*Mex3a*$^{+/-}$ mouse-derived tumoroids were smaller and showed a budded-shape population that was

essentially absent from the *Apc*$^{+/F}$;*Kras*$^{+/G12D}$;*Fabpl*$^{+/Cre}$ animal-derived tumoroids (Figure 11). These results suggest that although MEX3A is not absolutely required for CRC initiation, its reduced expression and/or function impacts tumor development *in vivo* and causes a change in tumoroid growth dynamics *ex vivo*.

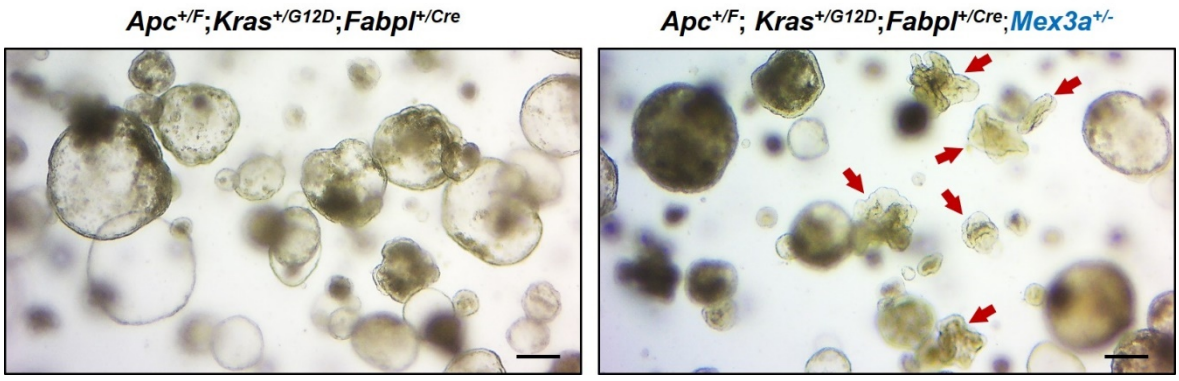

Figure 11| *Apc*$^{+/F}$;*Kras*$^{+/G12D}$;*Fabpl*$^{+/Cre}$ and *Apc*$^{+/F}$;*Kras*$^{+/G12D}$;*Fabpl*$^{+/Cre}$;*Mex3a*$^{+/-}$ tumoroids after 7 days of culture. Representative phase-contrast microscopy images of the size and morphology of tumoroids derived from CRC tissues of the two different mouse models. Budded structures are noticeable in the *Apc*$^{+/F}$;*Kras*$^{+/G12D}$;*Fabpl*$^{+/Cre}$;*Mex3a*$^{+/-}$ tumoroids (red arrows). Scale bar: 100 µm.

4.2. *Apc*$^{+/F}$;*Kras*$^{+/G12D}$;*Fabpl*$^{+/Cre}$;*Mex3a*$^{+/-}$ mouse-derived CRC tumoroids show increased sensitivity to PPARγ pathway activation

The reduced tumor burden in *Apc*$^{+/F}$;*Kras*$^{+/G12D}$;*Fabpl*$^{+/Cre}$;*Mex3a*$^{+/-}$ mice and the altered morphology of their derived CRC tumoroids might indicate an alteration in the cancer cells differentiation balance. Previously, we showed that MEX3A expression in murine ISCs represses the PPARγ pathway critically contributing to intestinal homeostasis by the increase of target genes involved in cellular differentiation (Pereira et al., 2020). Thus, we decided to evaluate the possible involvement of the PPARγ pathway in this cancer context.

Tumoroid cultures were treated for 5 days with Rosiglitazone (ROSI), a PPARγ-selective agonist. We observed evident differences between the ROSI-treated and the vehicle (DMSO)-treated tumoroids. PPARγ activation led to an overall decrease in tumoroid size and to a significant reduction in the number of large cystic structures in both genotypes. Interestingly, the population of budded tumoroids became more noticeable, particularly in the *Apc*$^{+/F}$;*Kras*$^{+/G12D}$;*Fabpl*$^{+/Cre}$ tumoroids, resembling the morphological phenotype

observed in the *Apc*$^{+/F}$;*Kras*$^{+/G12D}$;*Fabpl*$^{+/Cre}$;*Mex3a*$^{+/-}$ DMSO-treated (and non-treated) tumoroids (Figure 12).

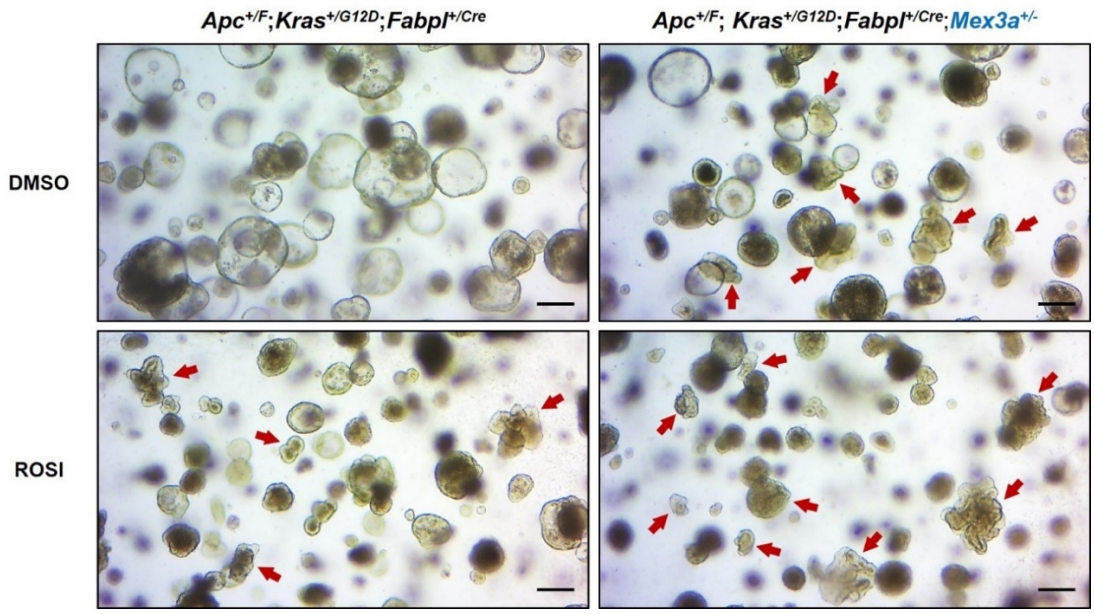

Figure 12 | *Apc*$^{+/F}$;*Kras*$^{+/G12D}$;*Fabpl*$^{+/Cre}$ and *Apc*$^{+/F}$;*Kras*$^{+/G12D}$;*Fabpl*$^{+/Cre}$;*Mex3a*$^{+/-}$ tumoroids response to PPARγ agonist treatment. Representative phase-contrast microscopy images of tumoroid cultures in the presence of the PPARγ agonist ROSI and the drug vehicle DMSO after 5 days of treatment (7 days total in culture). Budded structures are highlighted (red arrows). Scale bar: 100 µm.

After treatment with the PPARγ agonist ROSI, we aimed to better understand the molecular effects on the tumoroid lines concerning their gene expression profile using quantitative real-time PCR to assess the expressions levels of specific ISC (*Axin2*, *Lgr5*, *Lrig1*), proliferation (*Pcna*), and differentiation (*Angptl4*) markers (Figure 13). We observed that *Apc*$^{+/F}$;*Kras*$^{+/G12D}$;*Fabpl*$^{+/Cre}$;*Mex3a*$^{+/-}$ (DMSO-treated) tumoroids present a significant decrease in expression of the ISC marker *Lgr5* and an increased expression of the PPARγ transcriptional target *Angptl4*, when compared to the *Apc*$^{+/F}$;*Kras*$^{+/G12D}$;*Fabpl*$^{+/Cre}$ (DMSO-treated) tumoroids. As expected, ROSI treatment stimulated the expression of *Angptl4*, indicating high activation levels of PPARγ signaling in both genotypes. However, the response was accentuated in the *Apc*$^{+/F}$;*Kras*$^{+/G12D}$;*Fabpl*$^{+/Cre}$;*Mex3a*$^{+/-}$ ROSI-treated condition, showing much lower expression levels of the ISC markers *Lgr5* and *Lrig1*, when compared to the *Apc*$^{+/F}$;*Kras*$^{+/G12D}$;*Fabpl*$^{+/Cre}$ ROSI-treated tumoroids. No significant differences were detected concerning *Axin2* and *Pcna* expression levels among all samples.

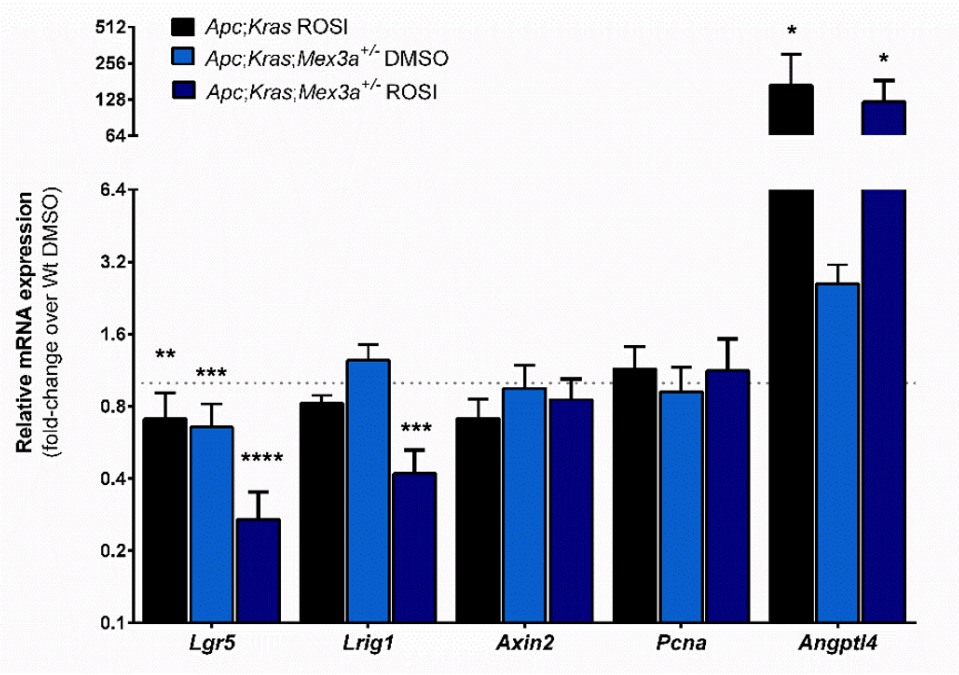

Figure 13 | Gene expression analyses by quantitative real-time PCR. Representative qPCR results of different expression levels of specific markers in tumoroids models. The tumoroid line *Apc*$^{+/F}$;*Kras*$^{+/G12D}$;*Fabpl*$^{+/Cre}$ treated with DMSO was used as the reference sample(dashed line). *P<0.05, **P= 0.0043, ***P < 0.001, ****P < 0.0001 Student's t-test.

These results indicate that tumor cells with decreased MEX3A expression show increased sensitivity to PPARγ pathway activation with consequent loss of stem cell potential and possibly an altered differentiation balance.

4.3. Functional evaluation of sgRNAs for *Trp53* KO by CRISPR-Cas9 technology

Having observed significant differences between CRC tumoroids growth and gene expression profile, we wanted to determine if the decreased stem cell potential in the context of MEX3A downregulation could somehow affect CIN onset. For that, we decided to introduce *Trp53* mutations by CRISPR/Cas9-mediated gene editing in the tumoroid models in order to generate compound mutants with p53 loss of expression to mimic advanced stages of CRC with genomic instability.

We proceeded with the cloning of the *Trp53* sgRNAs into the pSpCas9(BB)-2A-GFP expression vector and confirmed that two of them, sgRNA p53#4 and sgRNA p53#5, were correctly cloned into the vector (Figure 14). In parallel, we tested if the pSpCas9(BB)-2A-

GFP expression vector could be used for transfecting murine cells. We transfected the mouse fibroblast L cells with the empty vector and could observe about 10 to 15% GFP+ cells 48h after transfection (Figure 15A), indicating the plasmid was suitable for transfecting mouse-derived tumoroids. We then performed functional validation of the sgRNAs in L cells by transient transfection of each sgRNA construct and assessment of p53 protein expression by western blot. After 48 h of transfection, we could observe the presence of GFP+ cells to the same extent previously observed with the empty vector (Figure 15B). Western blot analysis showed that both sgRNA p53#4 and sgRNA p53 #5 were effective for p53 KO given the evident decrease in protein expression when compared to the control L cells. Protein quantification revealed an 45% decrease for sgRNA p53#4 and a 65% reduction for sgRNA p53#5 (Figure 15C). These results indicate that the sgRNAs worked adequately, even though there was a low yield concerning the number of transfected cells.

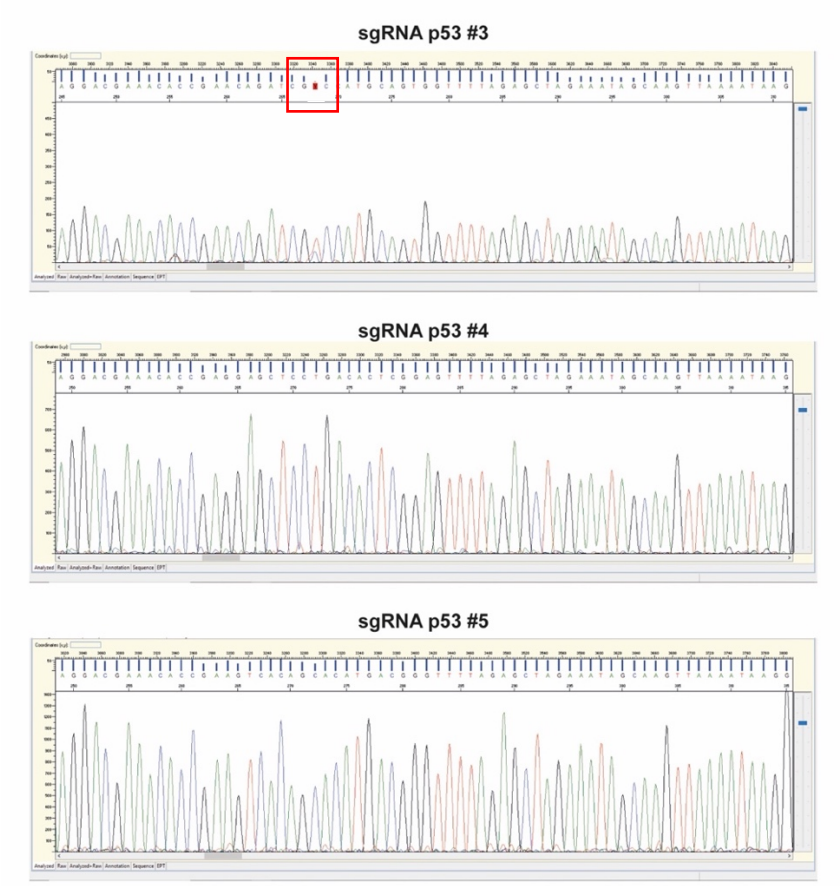

Figure 14 | Sanger sequencing electropherograms for the sgRNAs insertion site in PX458 vector. It was possible to verify that the sgRNA p53#4 and sgRNA p53#5 insertion between the U6 promoter and the sgRNA scaffold in PX458 was correct. For sgRNA p53#3, a nucleotide mismatch (in red) was observed and the sequence was discarded. Each peak represents a single nucleotide in different colors; A- green; T-red; C- blue: G- black.

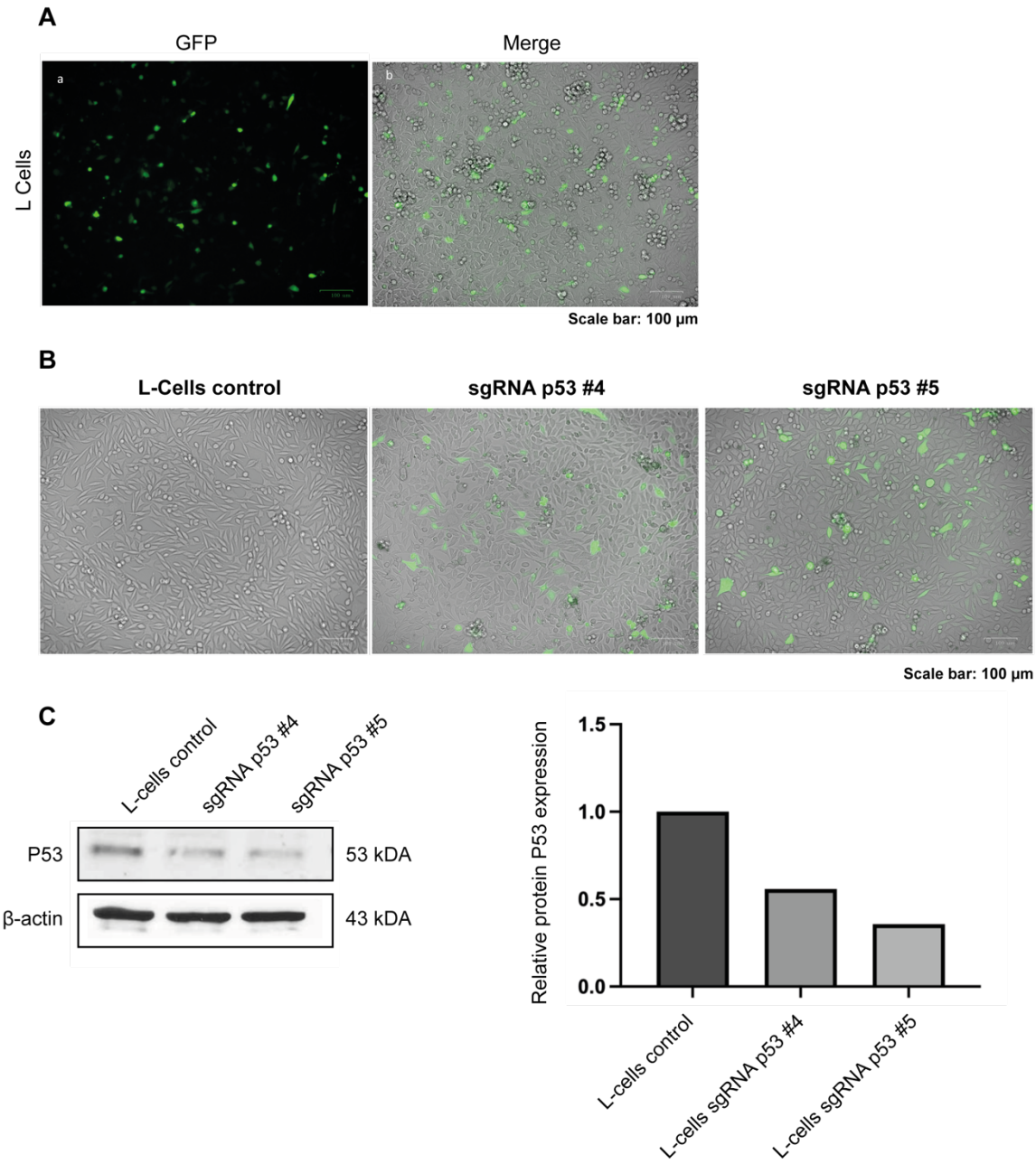

Figure 15 | Validation of sgRNAs against p53 in L-cells (A) Representative images of L cells 48 h after transient transfection with the empty vector PX458, showing fluorescence signals of GFP expression and suggesting the vector works in mice cells (merge is the overlay of the corresponding brightfield image and GFP expression). (B) L-cells transfected with sgRNA p53#4, and sgRNA p53#5 together with control (non-transfected) L cells are shown 48 h after transfection. Scale bar: 100 µm. (C) Western blot analysis for p53 expression and quantification values.

4.4. Establishment of *Trp53* KO CRC mouse tumoroids

Having validated sgRNAs for *Trp53* gene KO in L cells in standard (2D) cell culture conditions, we first tested the protocol for transfection of dissociated cells from the *Apc*$^{+/F}$;*Kras*$^{+/G12D}$;*Fabpl*$^{+/Cre}$ tumoroids using the PX458 empty vector. Overall, the transfection procedure resulted in a very low number of GFP+ 3D structures (Figure 16A). At this point, several steps were modified in order to optimize transfection conditions in this culture setting, namely: i) doubling the concentration of PX458 vector used for transfection and consequently the amount of lipofectamine; ii) decreasing cell density used for transfection; iii) introducing polybrene in the transfection mixture; iv) raising the time of incubation of cells with the transfection mixture. In the end, the optimization process only slightly improved the number of transfected structures (Figure 16B).

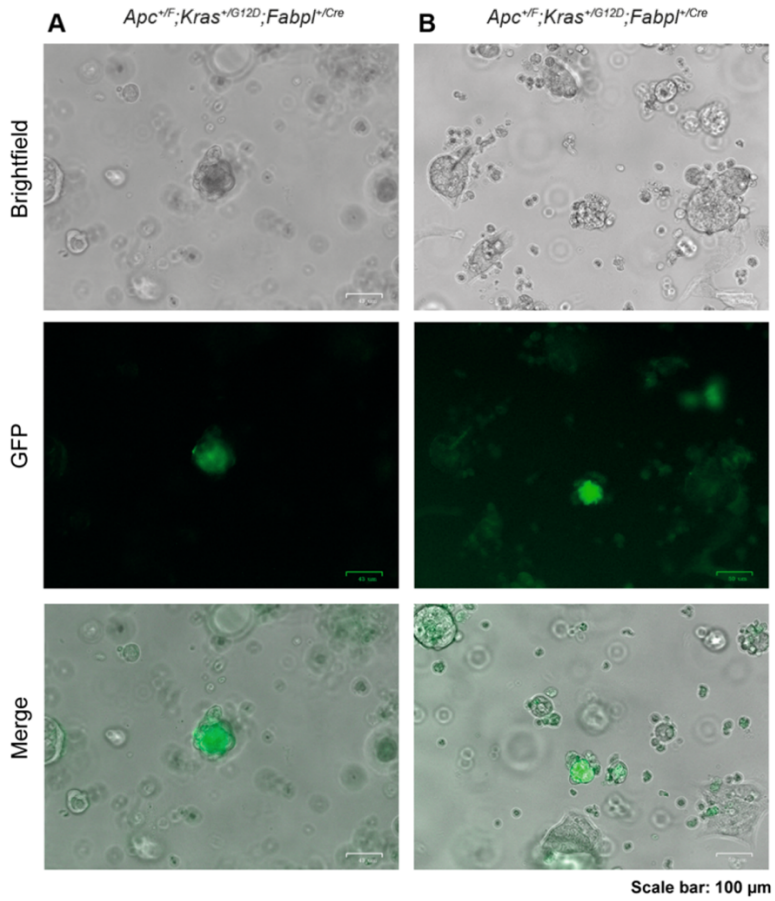

Figure 16 | Validation of the transfection protocol in *Apc*$^{+/F}$;*Kras*$^{+/G12D}$;*Fabpl*$^{+/Cre}$ tumoroids. Representative images of tumoroids (*Apc*$^{+/F}$;*Kras*$^{+/G12D}$;*Fabpl*$^{+/Cre}$) 48h after transfection with the empty vector PX458. The columns show two independent transfection protocols during the optimization process: A) before and B) after optimization. Scale bar: 100 µm.

We then proceeded with the transfection of the tumoroid cultures using the *Trp53* sgRNA constructs previously validated. Despite several attempts, we concluded that obtaining the *Trp53* KO CRC-derived tumoroids was a major challenge. Three days after each transfection, the tumoroids were subjected to selection by treatment with Nutlin-3a. Nutlin-3a is a small-molecule inhibitor of MDM2 that causes cell cycle arrest of non-edited cells (wild-type for p53 (Matano et al., 2015)). With successful p53 KO, it is expected that tumoroids became resistant to Nutlin-3a treatment, enabling functional selection for *Trp53* loss of function. We constantly observed that tumoroids could not survive or grow after drug selection. However, in our last attempt at the transfection protocol, we employed a new lipofectamine formulation (Lipofectamine 3000), which seems to be more suitable for genome editing applications, improving transfection efficiency and viability of difficult-to-transfect cells. Although the number of GFP+ structures following transfection was not higher than previously observed, we noticed that tumoroids were still growing after 5 days of treatment with Nutlin-3a and were able to passage them (Figure 17). We are now waiting to expand these cultures to collect material to confirm p53 KO by Western Blot and to use it for further experiments.

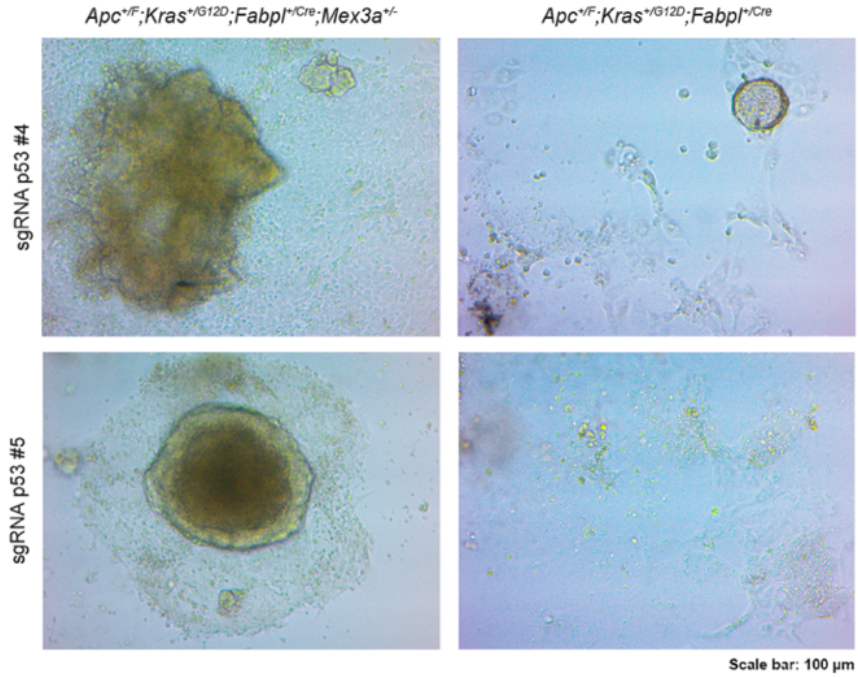

Figure 17 | Tumoroids *Apc*$^{+/F}$*;Kras*$^{+/G12D}$*;Fabpl*$^{+/Cre}$*;Mex3*$^{+/-}$ *and Apc*$^{+/F}$*;Kras*$^{+/G12D}$*;Fabpl*$^{+/Cre}$ growing after transfection and Nutlin-3a treatment. Each line of tumoroids was transfected using sgRNA p53#4 and sgRNA p53 #5. After Nutlin-3a treatment, the tumoroids are still growing. Scale bar: 100 µm.

4.5. Generation of MEX3A KO human tumoroids by CRISPR-Cas9 technology

As we wanted to develop a complementary study models, we started to use human tumoroids derived from CRC patients. Given the higher complexity level of human tumor tissues concerning genetic alterations, this was an opportunity to address the role of MEX3A in a context where CIN could already be present (more advanced tumor stages). For that, we decided to establish a *MEX3A* KO human tumoroid line by CRISPR/Cas9-mediated gene editing.

4.5.1. Establishment and characterization of human-derived CRC tumoroids

Having human tumoroids cultures already established, we started by evaluating their capacity to mimic the primary tumor phenotype. We compared the expression profile of a panel of cell lineage markers in the CRC tissue (adjacent normal-like and tumor tissues) from patient 007 and its derived tumoroids cultured in the presence (007T Wnt) or absence (007T w/o Wnt) of WNT3A-CM, through different histological staining techniques.

Concerning the normal-like tissue adjacent to tumor, all the markers tested showed the expected expression pattern for a normal colonic mucosa (Figure 18 and Figure 19, 007N Colon tissue panel). It was possible to see few nuclei positive for β-catenin at the crypts base, indicating active Wnt signaling, and in the first third of the crypt staining for the proliferation marker KI67, showing an active TA population. Alcian Blue staining showed the presence of goblet cells (in blue) along the crypts and cytokeratin-20 (CK20) was detected only in the upper (most differentiated) part of the colonic crypts. Regarding PPARγ, it showed ubiquitous nuclear expression along the normal crypts. On the other hand, p53 expression was barely detected in the normal tissue, with very few cells showing nuclear staining (possibly ongoing DNA damage). Regarding ISC markers, both *LGR5* and *MEX3A* mRNAs were detected at the base of the colonic crypts.

On the other hand, the expression profile obtained for the tumor tissue was very different (Figure 18 and Figure 19, 007T Colon Tissue). HE staining exhibited typical glandular architecture loss. Abnormal Wnt signaling was observed by the increased nuclear expression of β-Catenin, as well as an increased proliferative potential indicated by the

presence of KI67+ cells. Concomitantly, Alcian Blue staining revealed an almost complete absence of the differentiated goblet cell population, though CK20 expression was still retained. A strong decrease in PPARγ expression was observed, while p53 expression remained very low in a pattern similar to the one observed in the normal tissue. Concerning the ISC markers, a strong increase in the expression of *LGR5* was observed in the tumor tissue, while *MEX3A* expression remained relatively low.

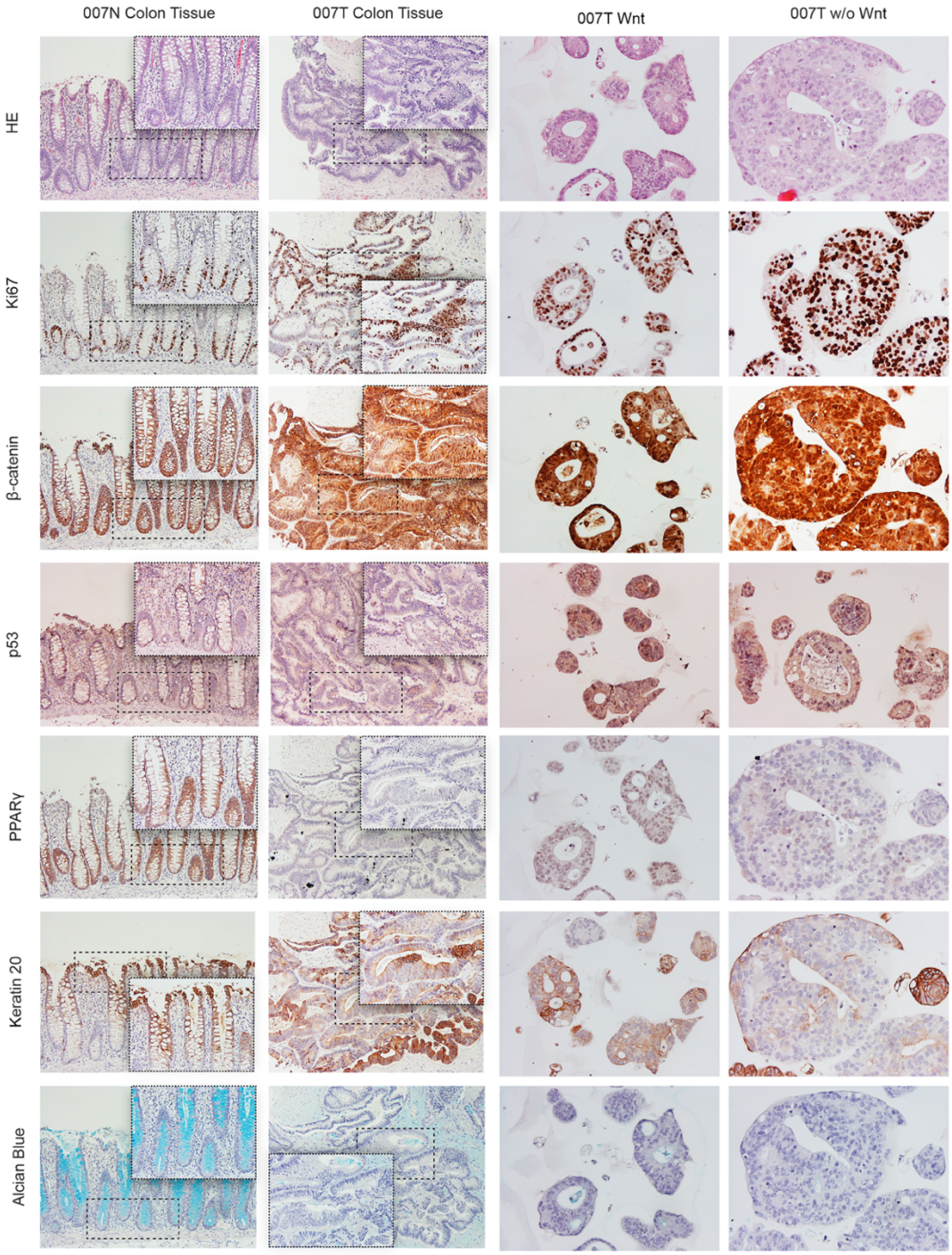

Figure 18 | Characterization of normal colon and CRC tissue of patient 007 and respective tumoroids. Representative HE (first row) images of normal colon tissue (007N), CRC tissue (007T) and tumoroids (007T Wnt and 007T w/o Wnt). Immunohistochemistry staining for proliferation marker KI67 (second row), Wnt pathway coactivator β-catenin (third row), tumor suppressor p53 (fourth row), differentiation pathway receptor PPARγ (fifth row), the intestinal differentiation marker CK20 (sixth row), and AB-PAS staining (seventh row). First two columns magnification: 100x; Boxes magnification: 200x; Tumoroids magnification: 200x.

Interestingly, when comparing the 007T tissue with its derived tumoroids (Figure 18 and Figure 19, 007T Wnt and 007T w/o Wnt), we could observe a similar expression profile pattern for most of the tested markers. Tumoroids exhibited similar increased expression of β-Catenin and KI67, loss of Alcian Blue staining and heterogenous expression of CK20. PPARγ staining was also strongly reduced and p53+ cells not frequently detected. Regarding the ISC markers, the strong expression level of *LGR5* and low expression level of *MEX3A* were replicated in the tumoroids, when compared to the normal tissue. Even though we could not establish normal organoids derived from this patient and despite the fact that there seems to be few differences in terms of expression level for some markers between tumoroids cultured with or without WNT3A-CM (p.e., PPARγ and *LGR5* mRNA), overall, the tumoroids profile is quite comparable to the native tumor tissue, validating our culture conditions.

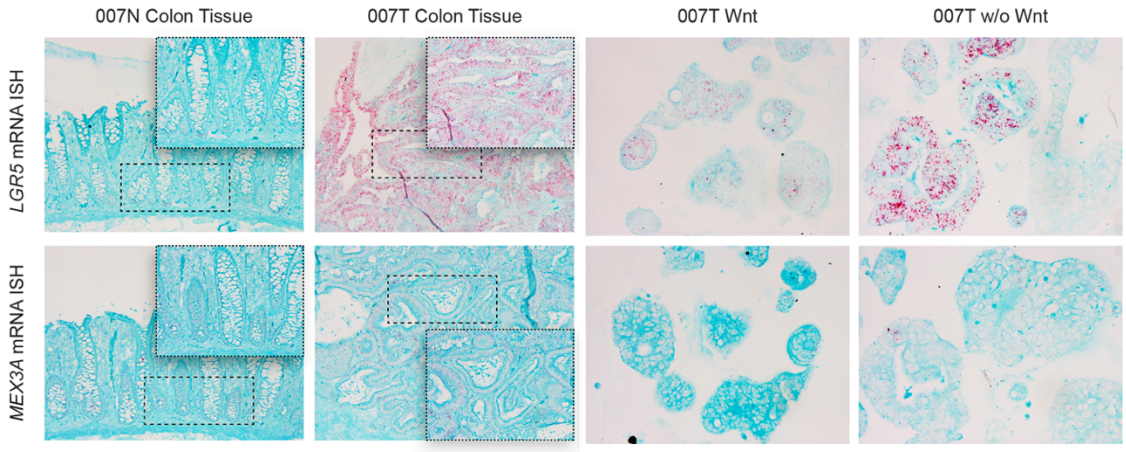

Figure 19 | mRNA ISH for *MEX3A* and *LGR5* in 007N tissue, 007T tissue, 007T Wnt, and 007T without Wnt. Boxes indicate magnified regions in the stained tissue. First two columns magnification: 100 x; Boxes magnification: 200 x; Tumoroids magnification: 200x.

Having validated our tumoroid culture conditions in terms of replicating the expression profile of specific markers in the primary tumor tissue, we started to characterize other cultures derived from CRC patients.

In this instance, we were able to establish a normal colon organoid line derived from patient 005 (005N) to be used as a control. 005N organoids showed a similar profile to the 007N colon tissue regarding the different markers tested. On the other hand, tumoroids derived from patients 005 (005T Wnt and 005T w/o Wnt) and 010 (010T w/o Wnt) showed increased Wnt signaling as observed by strong nuclear β-catenin expression and higher number of KI67+ proliferating cells (Figure 20). At the same time, we observed decreased expression of CK20 and Alcian Blue staining in all tumoroid conditions compared to 005N, even though 010T tumoroids retained CK20 expression (Figure 21). PPARγ staining was strongly reduced in 005T but not in 010T, which showed expression levels comparable to 005N. Nuclear p53 expression was observed in tumoroids, particularly in the 005T line, possibly indicating altered p53 signaling. Regarding the ISC markers, strong expression of both *LGR5* and *MEX3A* were observed in tumoroids when compared to 005N (Figure 22).

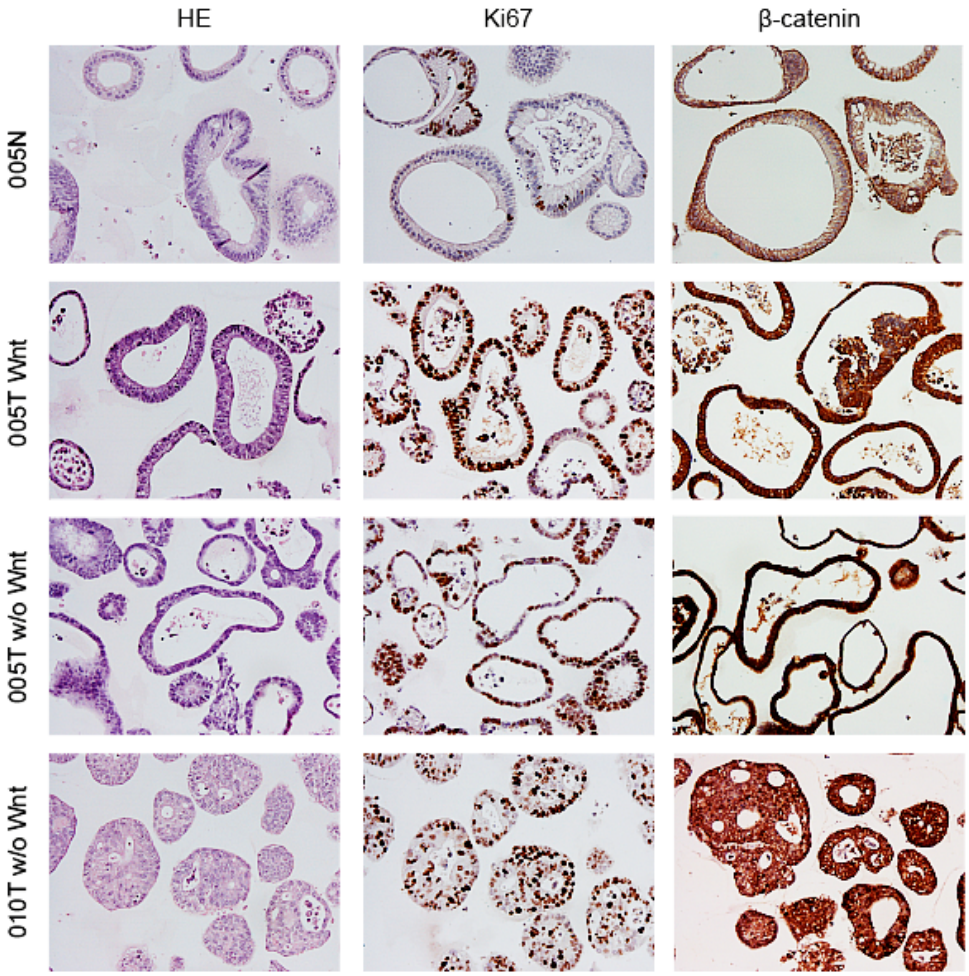

Figure 20 | Correlation of expression patterns for different markers between organoids derived from patient 005 and tumoroids of patients 005 and 010. Representative HE images (first column), IHC staining for proliferation marker KI67 (second column), and Wnt pathway coactivator β-catenin (third column). Magnification: 200x.

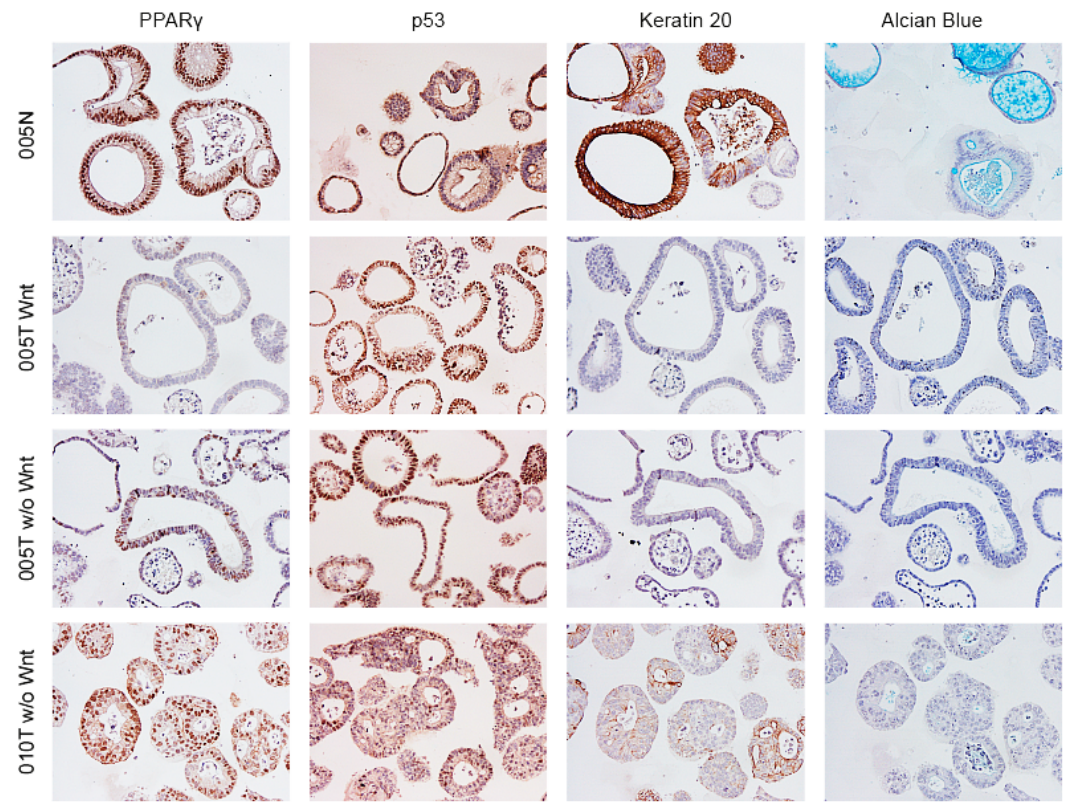

Figure 21 | Correlation of expression patterns for different markers between organoids derived from patient 005N and tumoroids of patients 005 and 010. Immunohistochemistry staining for differentiation pathway receptor PPARγ (first column), tumor suppressor gene p53 (second column) the intestinal differentiation marker CK20 (third column), and AB-PAS staining for secretory-cell differentiation evaluation (fourth column). All magnification: 200x.

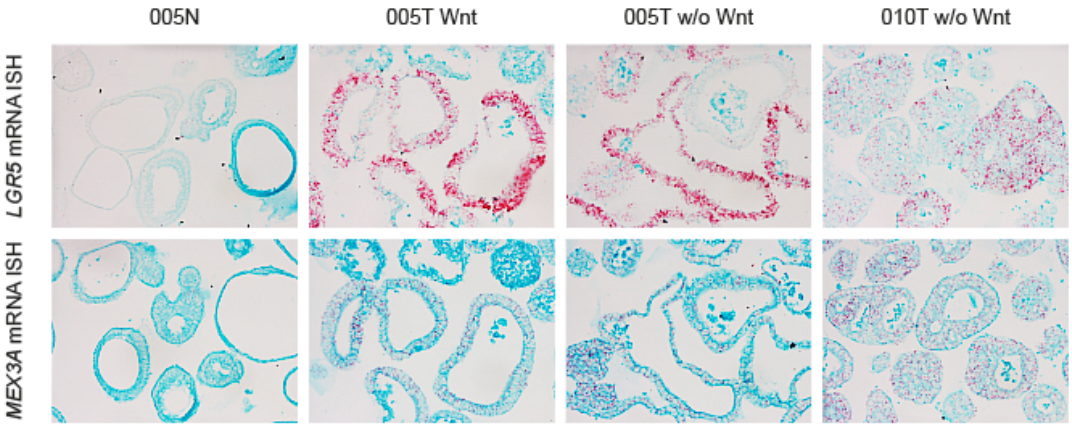

Figure 22 | mRNA ISH for MEX3A and LGR5 expression patterns markers between organoids derived from patient 005N and CRC-tumoroids of patients 005, and 010. On the upper panel there is the results for ISH *LGR5* mRNA and in the lower panel for *MEX3A* mRNA. All magnification: 200x.

4.5.2. Establishment of MEX3A KO tumoroids

In order to better characterize the MEX3A expression profile and its correlation with PPARγ, we evaluated the levels of MEX3A and PPARγ protein expression by Western Blot in the organoids and tumoroids from patient 005 (Figure 23). We confirmed that MEX3A was overexpressed in the 005T tumoroids when compared to 005N organoids. On the other hand, PPARγ expression was decreased in 005T tumoroids when compared to 005N organoids, reinforcing the inverse correlation in expression profile between both markers.

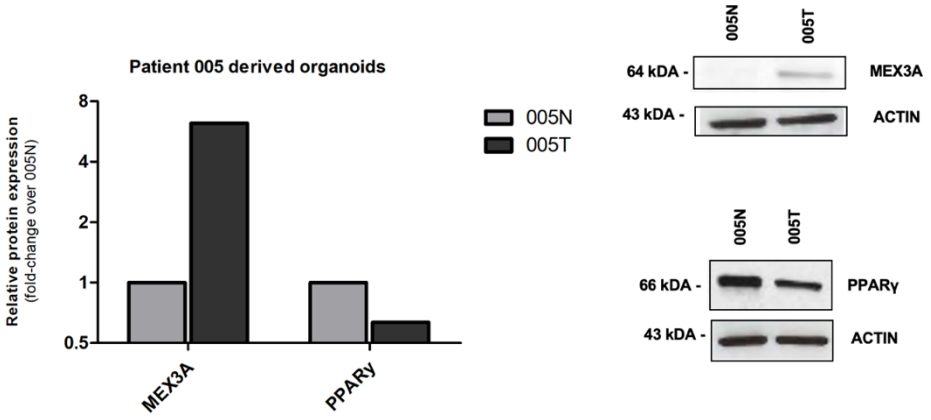

Figure 23 | Expression pattern of MEX3A and PPARγ on organoids and tumoroids of patient 005. The graph shows the Western blot analysis for MEX3A and PPARγ expression and their respective quantification values.

Having confirmed the overexpression of MEX3A protein levels in patient 005T, we decided to perform a MEX3A KO in this human-derived tumoroid line. Given the low yield of transfected cells previously obtained with the mouse tumoroids, we altered the transfection protocol, with two major changes: i) tumoroid cells were plated in collagen prior to transfection for higher availability towards the transfection vector; ii) as in this setting we could not use a drug-based selection approach, FACS was employed to isolate single cells expressing the GFP reporter. Using sgRNAs against *MEX3A* that had been previously validated in cell lines, we transfected 005T derived cells. Two days after transfection, the yield of GFP+ cells was relatively low (Figure 24A). Four days after transfection, FACS was performed to isolate cells expressing the GFP reporter, representing about 0,2% of the total number of cells (Figure 24B). Single cells were plated in collagen-coated 96-well plates to generate individual clones. Only three tumoroid lines survived the whole protocol and grew from a single cell till the culture reached the necessary confluence to be transferred to Matrigel (Figure 24C,a). In regular culture conditions, the tumoroids were expanded (Figure 24C,b), and material collected to confirm the MEX3A KO. Western Blot analyses confirmed

successful MEX3A KO, with the creation of a new tumoroid line named 005T Wnt AE6 (Figure 24D).

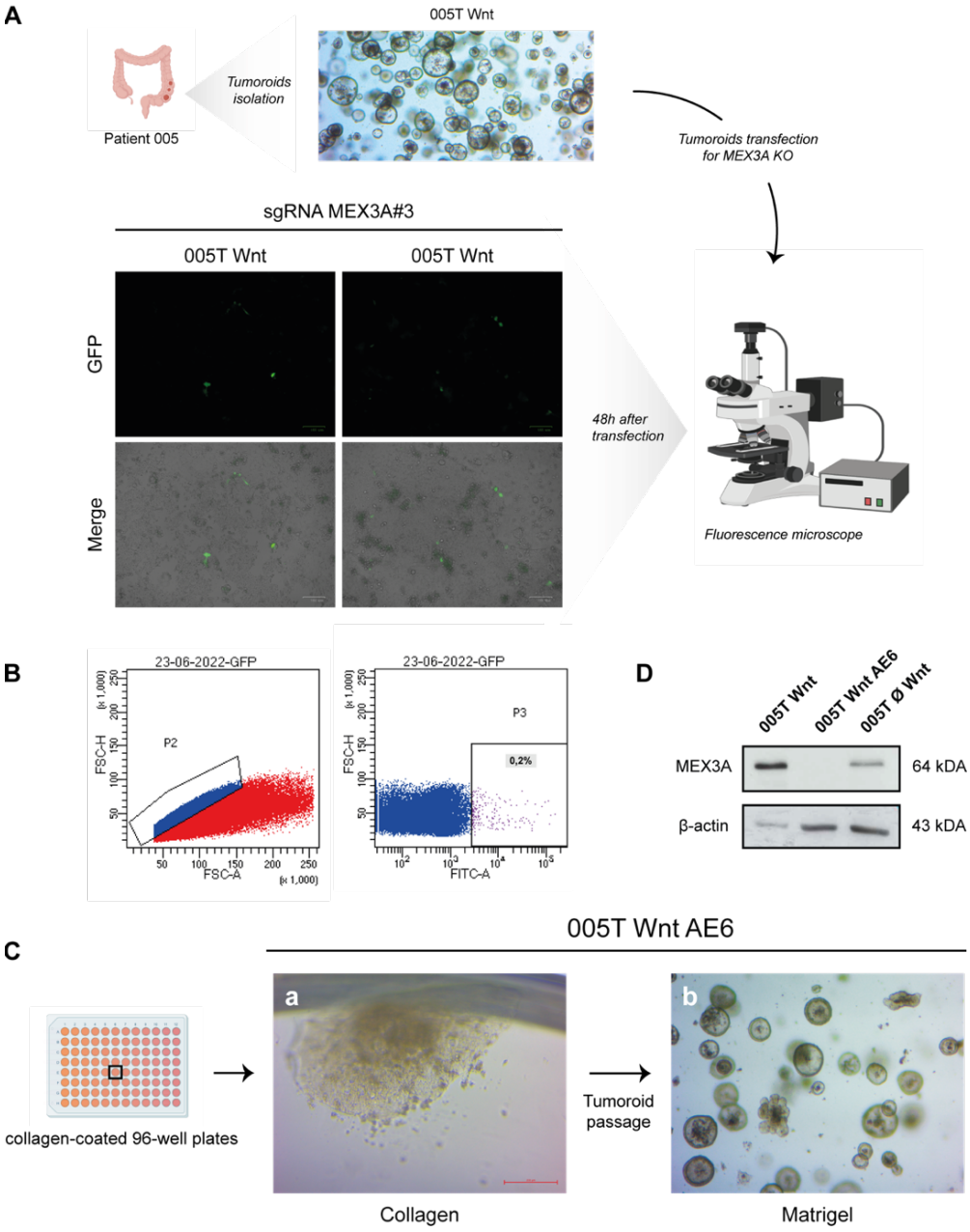

Figure 24 | Schematic view of the establishment of MEX3A KO tumoroids. A) Representative image of established human tumoroids (case 005T) used to perform the transfection protocol for MEX3A KO. The images were obtained 48 h after transfection using a fluorescence microscope, showing few cells expressing GFP. B) FACS results for GFP sorting, showed that only 0,2% of the cells expressed the GFP reporter C) After FACS, tumoroids were plated in single cells in a collagen-coated 96-well. The 005T Wnt AE6 clone is shown, growing in collagen (a). After weeks of growing in collagen, the tumoroids were passaged and plated in Matrigel for 14 days (b) (40x). D) Validation of MEX3A KO AE6 tumoroids by Western Blot technique.

4.5.3. Characterization of MEX3A KO tumoroids

Having the MEX3A KO model established and growing, we decided to characterize the cultures regarding the expression profile of the panel of cell lineage markers previously studied to investigate the impact of the MEX3A KO in human-derived tumoroids.

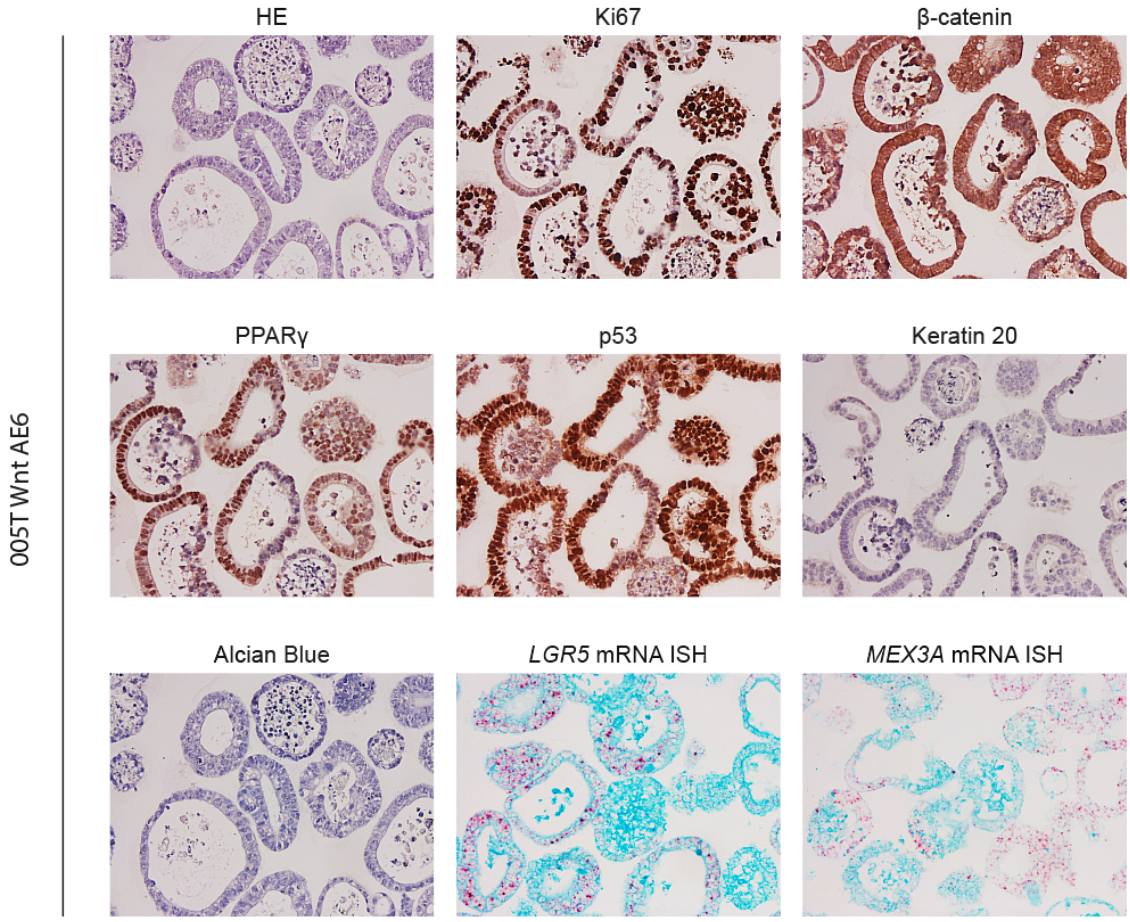

Figure 25 | Characterization of 005T Wnt AE6 tumoroids. Representative HE and IHC for proliferation marker KI67, Wnt pathway coactivator β-catenin, differentiation pathway receptor PPARγ, tumor suppressor p53, the intestinal differentiation marker CK20, AB-PAS and ISH for LGR5 mRNA and MEX3A mRNA. All magnification: 200x;

When compared to the 005T Wnt tumoroids we observed no difference in terms of nuclear β-catenin expression and KI67+ proliferating cells (Figure 25). Similarly, no difference was detected in terms of CK20 expression and Alcian Blue staining, which remained negative. However, a substantial increase was observed for PPARγ expression when compared to its isogenic control (compare Figure 21 and Figure 25). Interestingly, we found a correlation between PPARγ and p53 expression levels, with cells positive for PPARγ showing increased p53 expression. Moreover, MEX3A KO tumoroids presented a significant decrease in *LGR5*

mRNA expression compared to the 005T Wnt tumoroids (compare Figure 22 and Figure 25). *MEX3A* mRNA expression was still detected in the 005T Wnt AE6 tumoroids because the CRISPR/Cas9 approach used does not delete the mRNA sequence, but instead creates localized frameshift mutations that alter the sequence open reading frame.

To evaluate the impact of MEX3A loss in chromosome segregation fidelity, we analyzed mitotic errors using live-cell imaging. Despite several technical limitations regarding the confocal microscope setup, we were able to conduct some imaging experiments using non-toxic and cell-permeable fluorescent probes for DNA and microtubules. Cell divisions were analyzed and classified in four types of segregation errors: anaphase bridge, lagging chromosome, multipolar, or no error (Figure 26A). We did not observe any error during mitosis using a normal organoid cell line (001N; Figure 26B). On the other hand, chromosome segregation errors in tumoroids were observed in the 005T Wnt and the 005T Wnt AE6 (MEX3A KO). Lagging errors were however more frequent in 005T Wnt cells. Moreover, these cells exhibited longer mitotic duration (data not shown) and multipolar spindles were observed (n = 3). Overall, the results with the human-derived CRC tumoroids show that MEX3A impacts stem cell potential directly, as its loss leads to decreased *LGR5* expression and increased PPARγ activity. Moreover, loss of MEX3A expression might ameliorate CIN since we observed a decreased number of chromosome segregation errors.

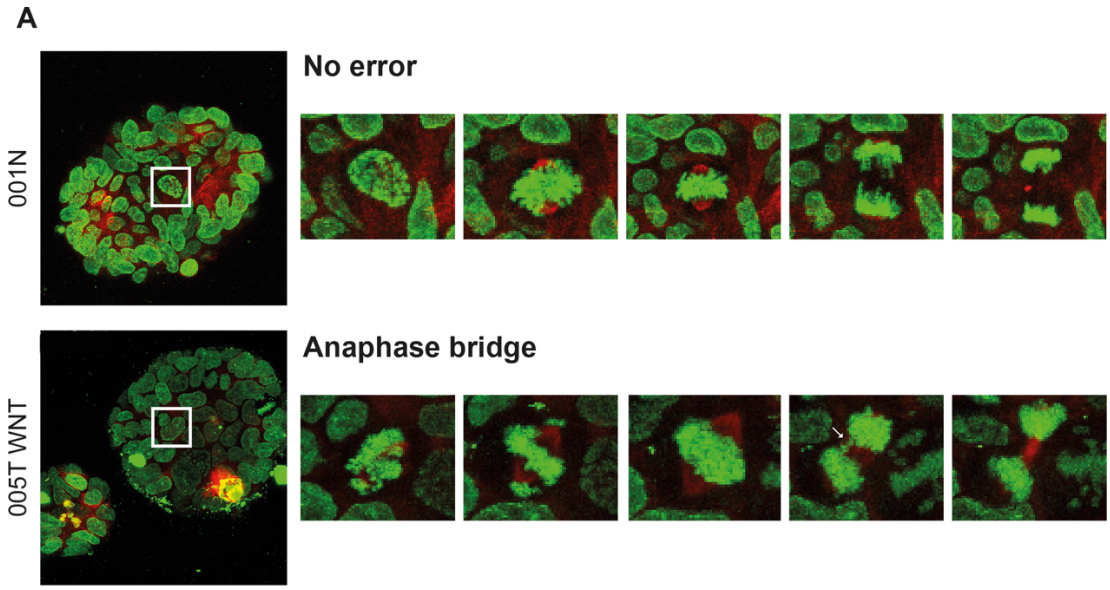

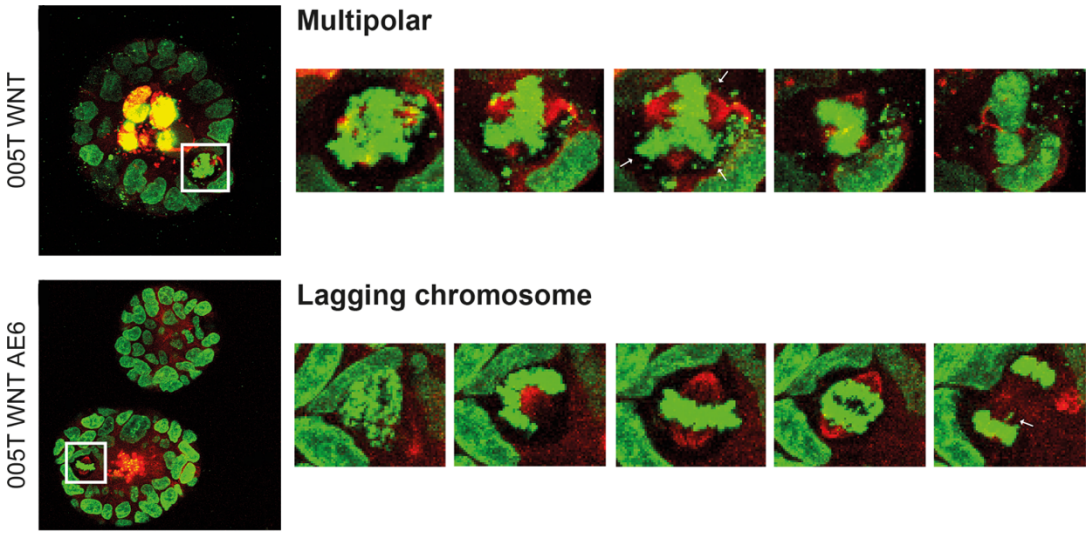

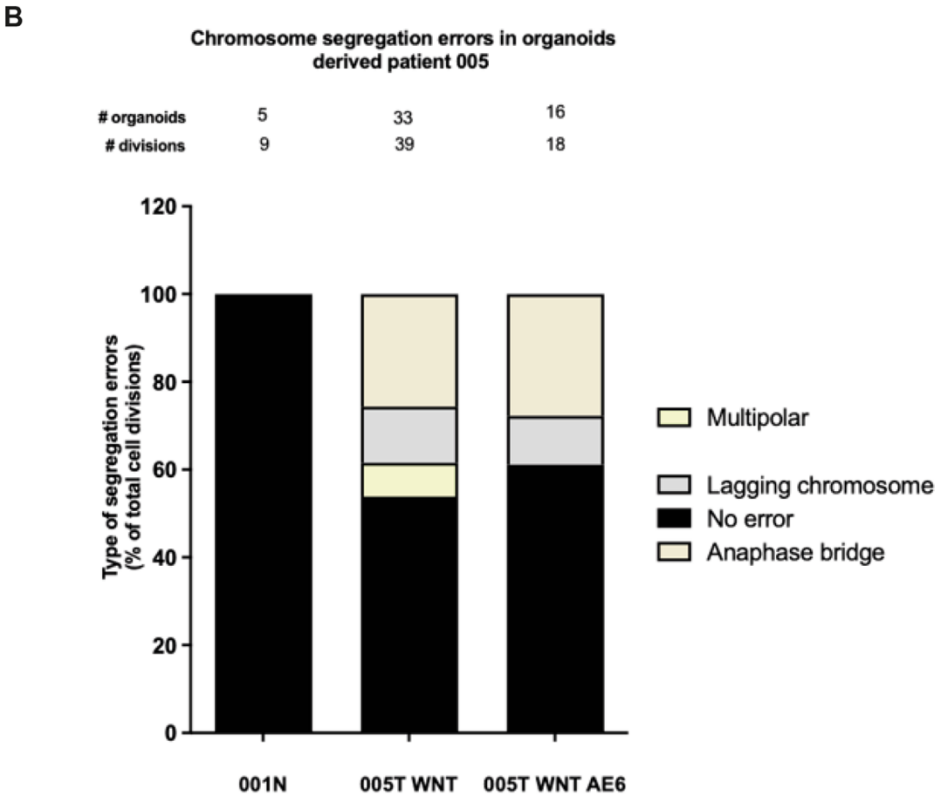

Figure 26 | Chromosome segregation errors in organoids. A) The panel shows representative images from live imaging of chromosome segregation during mitosis. Four segregation errors were analyzed: no error, anaphase bridge, multipolar, and lagging chromosome. DNA is stained by SPY505-DNA (green fluorescence) and microtubules by SPY555-tubulin (red fluorescence). The images were obtained in a x40 water immersion objective. B) Graph shows the percentage of each type of segregation error per organoid line. All the analysis was performed using ImageJ/Fiji software.

Chapter 5 | Discussion

CRC is a heterogeneous disease representing one of the most aggressive types of cancers in terms of worldwide mortality. Although several studies have been characterizing and identifying the mutation profile and pathways involved in this carcinogenic process, there it is still a lot to be discovered. RBPs, as part of the post-transcriptional regulatory machinery, can play a role in pathological conditions and have been gaining attention in the cancer field (Pereira et al., 2017). Nonetheless, the role of the RBP MEX3A, mainly involved in maintaining intestinal homeostasis, is still not fully addressed in the CRC context. Given MEX3A role in mediating ISC identity, we hypothesized that MEX3A might contribute to tumor cell heterogeneity in a context of CIN, the most frequent type of genetic instability observed in CRC. To address this, we established two complementary study models: 1) a murine CRC model with baseline MEX3A downregulation in which a p53 KO was created in order to potentially induce CIN; 2) a human CRC model with potential CIN in which a MEX3A KO was introduced. With this strategy we would be able to assess if reduced MEX3A expression makes CRC cells more refractory to develop CIN (early stage) and if CRC cells with CIN installed (late stage) become less aggressive upon MEX3A KO.

To first investigate the effects of reduced MEX3A expression in CRC, we used the *Apc*$^{+/F}$;*Kras*$^{+/G12D}$;*Fabpl*$^{+/Cre}$ and *Apc*$^{+/F}$;*Kras*$^{+/G12D}$;*Fabpl*$^{+/Cre}$;*Mex3a*$^{+/-}$ mice. These genetically engineered mouse models were a good option for studying the effects over CRC since they were expected to develop cancer in few weeks mimicking early stage human CRC (Haigis et al., 2008). We could observe that *Apc*$^{+/F}$;*Kras*$^{+/G12D}$;*Fabpl*$^{+/Cre}$;*Mex3a*$^{+/-}$ mice showed a decreased tumor burden in the distal colon when compared to *Apc*$^{+/F}$;*Kras*$^{+/G12D}$;*Fabpl*$^{+/Cre}$ animals. A change in mouse-derived tumoroids growth and shape was also observed, with the presence of a budded-shape population in *Apc*$^{+/F}$;*Kras*$^{+/G12D}$;*Fabpl*$^{+/Cre}$;*Mex3a*$^{+/-}$ derived tumoroids that was essentially absent in the *Apc*$^{+/F}$;*Kras*$^{+/G12D}$;*Fabpl*$^{+/Cre}$ derived tumoroids. Interestingly, these budding structures are reminiscent of normal colonic organoids (Sato, Stange, et al., 2011), indicating MEX3A was impacting differentiation patterns. We could not study the impact of full MEX3A loss with the characterization of *Apc*$^{+/F}$;*Kras*$^{+/G12D}$;*Fabpl*$^{+/Cre}$;*Mex3a*$^{-/-}$ mice because none was born, despite the occurrence of several litters. It is possible that the combined presence of *Apc*, *Kras* and *Mex3a* mutations is embryonically lethal, as also observed for half of the expected *Mex3a* homozygous mutants (Pereira et al., 2020). Nevertheless, our results indicated that

although MEX3A is not required for CRC initiation, its reduced expression directly impacts tumor development *in vivo*.

To gather more insights regarding the molecular mechanisms associated with the previous results, we treated the mouse-derived tumoroids with a PPARγ-selective agonist in order to explore the putative link between MEX3A and the PPARγ signaling pathway. The PPARγ pathway has been described as essential to promote lipid metabolism and differentiation and maintaining cell homeostasis. To test this hypothesis, we treated the mouse-derived tumoroid lines with ROSI, observing an increased sensitivity to PPARγ pathway activation in the *Apc*$^{+/F}$;*Kras*$^{+/G12D}$;*Fabpl*$^{+/Cre}$;*Mex3a*$^{+/-}$ when compared to *Apc*$^{+/F}$;*Kras*$^{+/G12D}$;*Fabpl*$^{+/Cre}$. These results indicate that tumors with decreased MEX3A expression show increased PPARγ pathway activation under treatment. Quantitative real-time PCR highlighted the possible loss of stem cell potential in *Mex3a*$^{+/-}$ tumoroids models under this treatment, verified by lower expression levels of *Lgr5* and *Lrig1*. These results are in line with our previous work and other published papers reporting the correlation between *Lgr5*+ and MEX3A levels (Barriga et al., 2017; Pereira et al., 2020). Interestingly, the proliferation marker *Pcna* did not vary between samples, even though ROSI treatment seems to affect tumoroid size. A possible explanation for this finding is that the mice tumoroids used in the study continue to have an activating *Kras* mutation that constitutively promotes cell proliferation, explaining the persistently high levels of the proliferation marker, as reported in pancreatic cancer models (Ischenko et al., 2021). Another hypothesis is that evaluating *Pcna* at the mRNA level is not the best approach to evaluate the proliferation status of tumoroids. We will evaluate proliferation status by looking at KI67 expression through immunohistochemistry staining.

To potentially increase CIN levels, we performed a transient transfection protocol through CRISPR-Cas9 to introduce a p53 KO in the mouse-derived CRC tumoroids. The optimization of this protocol proved to be a challenging task. In all attempts, the process resulted in low-yield transfected cells expressing the GFP reporter. Consistent results have been reported to support the low efficiency of organoids/tumoroids transfection protocols (Matano et al., 2015). Recent studies show that lentiviral vectors are better suited to genetically edit 3D cell cultures, improving the yield (Maru et al., 2016). Nevertheless, by altering some conditions, including the addition of polybrene, which has been described to enhance transfection efficiency in mammalian cells (Abe et al., 1998) and changing from Lipofectamine 2000 to the newest formulation Lipofectamine 3000, reported to be a better

option for hard to transfect cells, exhibited a slight improvement in the number of transfected cells.

The second challenge with the establishment of the p53 KO model was cell selection by treatment with the nongenotoxic drug Nutlin-3a. This drug works as a potent small-molecule inhibitor of MDM2 protein, an important protein responsible for binding p53 and marking it for proteasomal degradation. When MDM2 binds to Nutlin-3a, p53 is stabilized and the p53 pathway is activated, originating cell cycle arrest or apoptosis of p53 wild-type cells (De Sousa E Melo et al., 2017; Matano et al., 2015). Tumoroids did not grew after Nutlin-3a treatment, except for in our last attempt, when tumoroids were kept in culture after exposure to Nutlin-3a for several days, indicating that we might have established a p53 KO line. However, we are currently waiting to expand the cultures to proceed with the analyses to confirm the results. We also speculate that the protocol we have established for MEX3A KO in human-derived CRC tumoroids might work better for p53 KO in mouse tumoroids and will test this in the near future.

Following our objective of addressing the role of MEX3A in more advanced lesions, where CIN could already be in place, we processed tissue samples from patients with CRC to establish human-derived tumoroids. Each case has a mutational signature dictating a strict dependence on specific signaling pathways, so we employed niche modulation to promote tumor cell-selective growth. Thus, cells were cultured in the presence and absence of WNT3A-CM. When cells present mutations in the Wnt/β-catenin pathway (the first and most common alteration in CRC), tumoroid growth becomes independent of the presence of Wnt ligands in the culture medium (Sato et al., 2009). This modulation of the culture medium (absence of WNT3A-CM) allowed us to select for tumor cells only, and since tumoroids grew in this condition it indicates that all cases tested have mutations in the Wnt/β-catenin pathway. Nonetheless, the next step will be to confirm and extend in more depth the mutational profile for each tumoroid line through targeted DNA sequencing.

While establishing human tumoroid lines, we first evaluated if the tumoroids in our culture conditions mimicked tumor tissue conditions, as previously indicated (Kim et al., 2020). We demonstrated by histological analyses that tumoroids derived from patient 007 mimic the expression profile observed in the primary tumor tissue for all the markers tested. The ISH results for *MEX3A* mRNA exhibited low levels of *MEX3A* expression in the tumor tissue. In our ongoing work, we have observed that about 25% of human CRC cases show low MEX3A expression levels (or do not express it), and this could be one such case. The

characterization of the different tumoroid lines revealed an increase in expression of both *MEX3A* and *LGR5* and a decreased expression of PPARγ (except in 010T tumoroids) when compared to normal colonic organoids or normal colon tissue. Overall, this inverse correlation reinforces the data observed in the mouse models.

As transfecting tumoroids to establish a p53 KO proved to be a challenging task, we further optimized the protocol to successfully create a MEX3A KO in human-derived tumoroids (005T Wnt AE6). In this model we observed a decrease in *LGR5* mRNA expression together with a significant increase in PPARγ expression when compared to its isogenic control (005T Wnt). This result provides functional evidence of the role of MEX3A in directly regulating LGR5 expression and the PPARγ pathway, especially because this model retains the same mutational profile (including mutations in the Wnt/β-Catenin pathway) of the parental 005T line. Overall, the results observed in the KO are in accordance with our statistically significant correlation observed in human CRC cases, where high levels of MEX3A (85% of cases) correlate with low levels of PPARγ (75% of cases). Another interesting observation was the fact that PPARγ and p53 expression seem to overlap, with cells positive for PPARγ showing increased p53 expression. It has been previously described that PPARγ signaling is also involved in cell cycle control, including G1/S transition, where p53 acts as the main regulator (Han et al., 2003). This might have implications for the level of genetic instability in the cells. In fact, it has been shown that PPARγ signaling might influence the expression of genes controlling the DNA damage response under inflammatory conditions (Mierzejewski et al., 2022), including Growth-Arrest and DNA-Damage inducible 45 beta (*GADD45β*), which plays an important role in G2/M arrest, and Ataxia Telangiectasia Mutated (*ATM*) kinase, which acts as a master regulator of the cellular response to DNA DSBs regulating p53 among other proteins. To clarify this correlation, future experiments are needed, which might include treating the MEX3A KO with a PPARγ-selective antagonist to explore if there is a decrease in p53 expression in the KO and addressing the implications in terms of CIN levels.

To try and directly assess the impact of MEX3A loss over the CIN phenotype, we performed live-cell imaging of tumoroids lines to observe cell divisions and classify chromosome segregation errors (Bolhaqueiro et al., 2019). For the murine tumoroids with p53 KO we have not yet confirmed the establishment of the model, and so the evaluation of mitotic errors in a context of ensuing CIN will be evaluated in the future. Still we were able to perform a preliminary analysis using the MEX3A KO model in order to assess if in more

advanced tumor stages, MEX3A modulation might have an impact over the instability phenotype. This also proved to be a challenging task, as we could not yet obtain a significant number of dividing cells for analysis due to technical difficulties in optimizing the live imaging setup. These include limitations related with the microscope objective working distance, a particular problem for thicker samples (like organoids growing in a 3D matrix) and total duration of the experiment, which was limited to 3h for each recording session due to water evaporation while using a x40 water immersion objective (required continuous reposition of water, which led to an interruption in the acquisition of images of ongoing mitosis). Such limitations can be partially surpassed by optimizing the cell/Matrigel suspension to a very thin layer and using an objective with a water immersion micro dispenser automatized system, which will enable filming during longer periods of time. Despite these issues, our preliminary data showed that the MEX3A KO clone (005T Wnt AE6) did not undergo multipolar errors and had a slight reduction in the number of chromosome segregation errors when compared to the parental line (005T Wnt), which might indicate an attenuation of the CIN phenotype. This, however, requires further validation. Moreover, it would be interesting to employ a panel of tumoroid lines with different degrees of CIN and correlate this with the functional impact of MEX3A loss.

During mitosis, the spindle assembly checkpoint (SAC) is a surveillance mechanism that delays anaphase onset until all chromosomes are correctly attached to spindle microtubules, thus preventing chromosome missegregation. MPS1 is a key SAC regulator and it is often upregulated in colorectal tumors (Diogo et al., 2017). In this context, as 005T Wnt tumoroids present increased mitotic duration (data not shown), we speculate that proteins like MPS1 might be overexpressed in this model as well. However, this hypothesis needs further investigation in the future to assess the expression levels of SAC proteins that could influence the CIN+ phenotype for each patient. Nevertheless, our preliminary results allowed us to understand the optimal live-cell imaging conditions for future work. Although the correlation between MEX3A levels and the CIN phenotype for both models is still unclear our results illustrate the potential of using the 3D tumoroid culture model to address the molecular basis of genetic instability (Bolhaqueiro et al., 2019).

Chapter 6 | Future perspectives and concluding remarks

Considering the results obtained in this work, we concluded that the RBP MEX3A plays an important role in CRC carcinogenesis, as demonstrated by our results with *Mex3a*$^{+/-}$ heterozygous CRC mouse models exhibiting lower tumor burden *in vivo*, abnormal tumoroid growth and morphology *ex vivo* and an altered gene expression pattern, particularly concerning *Lgr5* and PPARγ signaling activity, indicating altered stem cell potential. This conclusion is further supported and extended by the impact of the loss of the MEX3A observed in the human-derived MEX3A KO tumoroids.

This work also sustains that MEX3A function directly impacts the PPARγ pathway, as observed in the human MEX3A KO tumoroid line. Although, future work will focus on the analysis of the MEX3A KO line, especially to study the possible correlation observed between PPARγ and p53 protein expression.

The link between MEX3A and the impact on chromosomal instability is still unclear. In future work, it will be necessary to increase the number of cell divisions analyzed and recording time of each tumoroid line during live-cell imaging to better investigate this association. This will allow us to obtain high confidence regarding the classification of chromosome segregation errors and provide a clearer answer regarding the possible association between MEX3A expression, genetic instability levels and consequently its impact over CRC behavior.

References

Abe, A., Miyanohara, A., & Friedmann, T. (1998). Polybrene increases the efficiency of gene transfer by lipofection. *Gene Therapy*, *5*(5), 708–711.

Amersi, F., Agustin, M., & Ko, C. Y. (2005). Colorectal Cancer: Epidemiology, Risk Factors, and Health Services. *Clinics in Colon and Rectal Surgery*, *18*(3), 133–140.

Araghi, M., Soerjomataram, I., Bardot, A., Ferlay, J., Cabasag, C. J., Morrison, D. S., De, P., Tervonen, H., Walsh, P. M., Bucher, O., Engholm, G., Jackson, C., McClure, C., Woods, R. R., Saint-Jacques, N., Morgan, E., Ransom, D., Thursfield, V., Møller, B., … Arnold, M. (2019). Changes in colorectal cancer incidence in seven high-income countries: a population-based study. *The Lancet. Gastroenterology & Hepatology*, *4*(7), 511–518.

Arnold, M., Sierra, M. S., Laversanne, M., Soerjomataram, I., Jemal, A., & Bray, F. (2017). Global patterns and trends in colorectal cancer incidence and mortality. *Gut*, *66*(4), 683–691.

Barker, N. (2014). Adult intestinal stem cells: critical drivers of epithelial homeostasis and regeneration. *Nature Reviews Molecular Cell Biology*, *15*(1), 19–33.

Barker, N., De Wetering, M. Van, & Clevers, H. (2008). The intestinal stem cell. *Genes & Development*, *22*(14), 1856–1864.

Barker, N., Ridgway, R. A., Van Es, J. H., Van De Wetering, M., Begthel, H., Van Den Born, M., Danenberg, E., Clarke, A. R., Sansom, O. J., & Clevers, H. (2009). Crypt stem cells as the cells-of-origin of intestinal cancer. *Nature*, *457*(7229), 608–611.

Barker, N., Van Es, J. H., Kuipers, J., Kujala, P., Van Den Born, M., Cozijnsen, M., Haegebarth, A., Korving, J., Begthel, H., Peters, P. J., & Clevers, H. (2007). Identification of stem cells in small intestine and colon by marker gene Lgr5. *Nature*, *449*(7165), 1003–1007.

Barker, N., Van Oudenaarden, A., & Clevers, H. (2012). Identifying the stem cell of the intestinal crypt: strategies and pitfalls. *Cell Stem Cell*, *11*(4), 452–460.

Barrangou, R., Fremaux, C., Deveau, H., Richards, M., Boyaval, P., Moineau, S., Romero, D. A., & Horvath, P. (2007). CRISPR provides acquired resistance against viruses in prokaryotes. *Science (New York, N.Y.)*, *315*(5819), 1709–1712.

Barriga, F. M., Montagni, E., Mana, M., Mendez-Lago, M., Hernando-Momblona, X., Sevillano, M., Guillaumet-Adkins, A., Rodriguez-Esteban, G., Buczacki, S. J. A., Gut, M., Heyn, H., Winton, D. J., Yilmaz, O. H., Attolini, C. S. O., Gut, I., & Batlle, E. (2017). Mex3a Marks a Slowly Dividing Subpopulation of Lgr5+ Intestinal Stem Cells. *Cell Stem Cell*, *20*(6), 801-816.e7.

Bédard, P., Gauvin, S., Ferland, K., Caneparo, C., Pellerin, È., Chabaud, S., & Bolduc, S. (2020). Innovative Human Three-Dimensional Tissue-Engineered Models as an Alternative to Animal Testing. *Bioengineering*, *7*(3), 115.

Bhanot, P., Brink, M., Samos, C. H., Hsieh, J. C., Wang, Y., Macke, J. P., Andrew, D., Nathans, J., & Nusse, R. (1996). A new member of the frizzled family from Drosophila functions as a Wingless receptor. *Nature*, *382*(6588), 225–231.

Bjerknes, M., & Cheng, H. (1981). The stem-cell zone of the small intestinal epithelium. I. Evidence from Paneth cells in the adult mouse. *The American Journal of Anatomy*, *160*(1), 51–63.

Bolhaqueiro, A. C. F., Ponsioen, B., Bakker, B., Klaasen, S. J., Kucukkose, E., van Jaarsveld, R. H., Vivié, J., Verlaan-Klink, I., Hami, N., Spierings, D. C. J., Sasaki, N., Dutta, D., Boj, S. F., Vries, R. G. J., Lansdorp, P. M., van de Wetering, M., van Oudenaarden, A., Clevers, H., Kranenburg, O., … Kops, G. J. P. L. (2019). Ongoing chromosomal instability and karyotype evolution in human colorectal cancer organoids. *Nature Genetics*, *51*(5), 824–834.

Buchet-Poyau, K., Courchet, J., Le Hir, H., Séraphin, B., Scoazec, J. Y., Duret, L., Domon-Dell, C., Freund, J. N., & Billaud, M. (2007). Identification and characterization of human Mex-3 proteins, a novel family of evolutionarily conserved RNA-binding proteins differentially localized to processing bodies. *Nucleic Acids Research*, *35*(4), 1289–1300.

Bufalieri, F., Caimano, M., Severini, L. L., Basili, I., Paglia, F., Sampirisi, L., Loricchio, E., Petroni, M., Canettieri, G., Santoro, A., D'angelo, L., Infante, P., & Di Marcotullio, L. (2020). The RNA-Binding Ubiquitin Ligase MEX3A Affects Glioblastoma Tumorigenesis by Inducing Ubiquitylation and Degradation of RIG-I. *Cancers*, *12*(2).

Burd, C. G., & Dreyfuss, G. (1994). Conserved structures and diversity of functions of RNA-binding proteins. *Science*, *265*(5172), 615–621.

Bürtin, F., Mullins, C. S., & Linnebacher, M. (2020). Mouse models of colorectal cancer: Past, present and future perspectives. *World Journal of Gastroenterology*, *26*(13), 1394–1426.

Cacciamali, A., Villa, R., & Dotti, S. (2022). 3D Cell Cultures: Evolution of an Ancient Tool for New Applications. *Frontiers in Physiology*, *13*, 1346.

Cano, F., Bye, H., Duncan, L. M., Buchet-Poyau, K., Billaud, M., Wills, M. R., & Lehner, P. J. (2012). The RNA-binding E3 ubiquitin ligase MEX-3C links ubiquitination with MHC-I mRNA degradation. *The EMBO Journal*, *31*(17), 3596–3606.

Cano, F., Miranda-Saavedra, D., & Lehner, P. J. (2010). RNA-binding E3 ubiquitin ligases: novel players in nucleic acid regulation. *Biochemical Society Transactions*, *38*(6),

1621–1626.

Cheng, H., & Leblond, C. P. (1974). Origin, differentiation and renewal of the four main epithelial cell types in the mouse small intestine. V. Unitarian Theory of the origin of the four epithelial cell types. *The American Journal of Anatomy*, *141*(4), 537–561.

Ciosk, R., DePalma, M., & Priess, J. R. (2006). Translational regulators maintain totipotency in the Caenorhabditis elegans germline. *Science (New York, N.Y.)*, *311*(5762), 851–853.

Clevers, H. (2006). Wnt/beta-catenin signaling in development and disease. *Cell*, *127*(3), 469–480.

Clevers, H. (2013). The intestinal crypt, a prototype stem cell compartment. *Cell*, *154*(2), 274–284.

Colnot, S., Niwa-Kawakita, M., Hamard, G., Godard, C., Le Plenier, S., Houbron, C., Romagnolo, B., Berrebi, D., Giovannini, M., & Perret, C. (2004). Colorectal cancers in a new mouse model of familial adenomatous polyposis: influence of genetic and environmental modifiers. *Laboratory Investigation; a Journal of Technical Methods and Pathology*, *84*(12), 1619–1630.

de Lau, W., Peng, W. C., Gros, P., & Clevers, H. (2014). The R-spondin/Lgr5/Rnf43 module: regulator of Wnt signal strength. *Genes & Development*, *28*(4), 305–316.

De Sousa E Melo, F., Kurtova, A. V., Harnoss, J. M., Kljavin, N., Hoeck, J. D., Hung, J., Anderson, J. E., Storm, E. E., Modrusan, Z., Koeppen, H., Dijkgraaf, G. J. P., Piskol, R., & De Sauvage, F. J. (2017). A distinct role for Lgr5+ stem cells in primary and metastatic colon cancer. *Nature*, *543*(7647), 676–680.

Diogo, V., Teixeira, J., Silva, P. M. A., & Bousbaa, H. (2017). Spindle Assembly Checkpoint as a Potential Target in Colorectal Cancer: Current Status and Future Perspectives. *Clinical Colorectal Cancer*, *16*(1), 1–8.

Draper, B. W., Mello, C. C., Bowerman, B., Hardin, J., & Priess, J. R. (1996). MEX-3 is a KH domain protein that regulates blastomere identity in early C. elegans embryos. *Cell*, *87*(2), 205–216.

Dreyfuss, G., Kim, V. N., & Kataoka, N. (2002). Messenger-RNA-binding proteins and the messages they carry. *Nature Reviews. Molecular Cell Biology*, *3*(3), 195–205.

Drost, J., & Clevers, H. (2018). Organoids in cancer research. *Nature Reviews Cancer*, *18*(7), 407–418.

Dubois, V., Eeckhoute, J., Lefebvre, P., & Staels, B. (2017). Distinct but complementary contributions of PPAR isotypes to energy homeostasis. *The Journal of Clinical*

Investigation, *127*(4), 1202–1214.

Fearon, E. R., & Vogelstein, B. (1990). A genetic model for colorectal tumorigenesis. *Cell*, *61*(5), 759–767.

Gao, F. J., Chen, J. Y., Wu, H. Y., Shi, J., Chen, M., Fan, X. S., & Huang, Q. (2014). Lgr5 over-expression is positively related to the tumor progression and HER2 expression in stage pTNM IV colorectal cancer. *International Journal of Clinical and Experimental Pathology*, *7*(4), 1572–1579.

Gebauer, F., Schwarzl, T., Valcárcel, J., & Hentze, M. W. (2021). RNA-binding proteins in human genetic disease. *Nature Reviews. Genetics*, *22*(3), 185–198.

Gerstberger, S., Hafner, M., & Tuschl, T. (2014). A census of human RNA-binding proteins. *Nature Reviews Genetics*, *15*(12), 829–845.

Glisovic, T., Bachorik, J. L., Yong, J., & Dreyfuss, G. (2008). RNA-binding proteins and post-transcriptional gene regulation. *FEBS Letters*, *582*(14), 1977–1986.

Haigis, K. M., Kendall, K. R., Wang, Y., Cheung, A., Haigis, M. C., Glickman, J. N., Niwa-Kawakita, M., Sweet-Cordero, A., Sebolt-Leopold, J., Shannon, K. M., Settleman, J., Giovannini, M., & Jacks, T. (2008). Differential effects of oncogenic K-Ras and N-Ras on proliferation, differentiation and tumor progression in the colon. *Nature Genetics*, *40*(5), 600–608.

Han, C., Demetris, A. J., Michalopoulos, G. K., Zhan, Q., Shelhamer, J. H., & Wu, T. (2003). PPARγ ligands inhibit cholangiocarcinoma cell growth through p53-dependent GADD45 and p21WAF1/Cip1 pathway. *Hepatology*, *38*(1), 167–177.

Hentze, M. W., Castello, A., Schwarzl, T., & Preiss, T. (2018). A brave new world of RNA-binding proteins. *Nature Reviews Molecular Cell Biology*, *19*(5), 327–341.

Hoevenaar, W. H. M., Janssen, A., Quirindongo, A. I., Ma, H., Klaasen, S. J., Teixeira, A., van Gerwen, B., Lansu, N., Morsink, F. H. M., Offerhaus, G. J. A., Medema, R. H., Kops, G. J. P. L., & Jelluma, N. (2020). Degree and site of chromosomal instability define its oncogenic potential. *Nature Communications*, *11*(1), 1501–1501.

Hooper, L. V., & MacPherson, A. J. (2010). Immune adaptations that maintain homeostasis with the intestinal microbiota. *Nature Reviews Immunology*, *10*(3), 159–169.

Huang, L., Malu, S., McKenzie, J. A., Andrews, M. C., Talukder, A. H., Tieu, T., Karpinets, T., Haymaker, C., Forget, M. A., Williams, L. J., Wang, Z., Mbofung, R. M., Wang, Z. Q., Davis, R. E., Lo, R. S., Wargo, J. A., Davies, M. A., Bernatchez, C., Heffernan, T., … Hwu, P. (2018). The RNA-binding Protein MEX3B Mediates Resistance to Cancer Immunotherapy by Downregulating HLA-A Expression. *Clinical Cancer Research : An Official Journal of the American Association for Cancer Research*, *24*(14), 3366–3376.

Hunter, C. P., & Kenyon, C. (1996). Spatial and temporal controls target pal-1 blastomere-specification activity to a single blastomere lineage in C. elegans embryos. *Cell*, *87*(2), 217–226.

IARC. (2022). *Colorectal Cancer Awareness Month 2022 – IARC*. https://www.iarc.who.int/featured-news/colorectal-cancer-awareness-month-2022/

Ischenko, I., D'Amico, S., Rao, M., Li, J., Hayman, M. J., Powers, S., Petrenko, O., & Reich, N. C. (2021). KRAS drives immune evasion in a genetic model of pancreatic cancer. *Nature Communications*, *12*(1), 1–15.

Ishino, Y., Krupovic, M., & Forterre, P. (2018). History of CRISPR-Cas from Encounter with a Mysterious Repeated Sequence to Genome Editing Technology. *Journal of Bacteriology*, *200*(7).

Ishino, Y., Shinagawa, H., Makino, K., Amemura, M., & Nakatura, A. (1987). Nucleotide sequence of the iap gene, responsible for alkaline phosphatase isozyme conversion in Escherichia coli, and identification of the gene product. *Journal of Bacteriology*, *169*(12), 5429–5433.

Jiang, H., Zhang, X., Luo, J., Dong, C., Xue, J., Wei, W., Chen, J., Zhou, J., Gao, Y., & Yang, C. (2012). Knockdown of hMex-3A by small RNA interference suppresses cell proliferation and migration in human gastric cancer cells. *Molecular Medicine Reports*, *6*(3), 575–580.

Jiang, S., Meng, L., Chen, X., Liu, H., Zhang, J., Chen, F., Zheng, J., Liu, H., Wang, F., Hu, J., & Li, Z. (2020). MEX3A promotes triple negative breast cancer proliferation and migration via the PI3K/AKT signaling pathway. *Experimental Cell Research*, *395*(2), 112191.

Jiao, Y., George, S. K., Zhao, Q., Hulver, M. W., Hutson, S. M., Bishop, C. E., & Lu, B. (2012). Mex3c mutation reduces adiposity and increases energy expenditure. *Molecular and Cellular Biology*, *32*(21), 4350–4362.

Johansson, M. E. V., Phillipson, M., Petersson, J., Velcich, A., Holm, L., & Hansson, G. C. (2008). The inner of the two Muc2 mucin-dependent mucus layers in colon is devoid of bacteria. *Proceedings of the National Academy of Sciences of the United States of America*, *105*(39), 15064–15069.

Kent, W. J., Sugnet, C. W., Furey, T. S., Roskin, K. M., Pringle, T. H., Zahler, A. M., & Haussler, and D. (2002). The human genome browser at UCSC. *Genome Research*, *12*(6), 996–1006.

Kim, J., Koo, B. K., & Knoblich, J. A. (2020). Human organoids: model systems for human biology and medicine. *Nature Reviews Molecular Cell Biology*, *21*(10), 571–584.

Kleist, B., Xu, L., Li, G., & Kersten, C. (2011). Expression of the adult intestinal stem cell marker Lgr5 in the metastatic cascade of colorectal cancer. *International Journal of Clinical and Experimental Pathology*, *4*(4), 327–335.

Knott, G. J., & Doudna, J. A. (2018). CRISPR-Cas guides the future of genetic engineering. *Science (New York, N.Y.)*, *361*(6405), 866–869.

Lauby-Secretan, B., Vilahur, N., Bianchini, F., Guha, N., & Straif, K. (2018). The IARC Perspective on Colorectal Cancer Screening. *New England Journal of Medicine*, *378*(18), 1734–1740.

Le Borgne, M., Chartier, N., Buchet-Poyau, K., Destaing, O., Faurobert, E., Thibert, C., Rouault, J. P., Courchet, J., Nègre, D., Bouvard, D., Albiges-Rizo, C., Rousseaux, S., Khochbin, S., Segretain, D., Crépieux, P., Guillou, F., Durand, P., Perrard, M. H., & Billaud, M. (2014). The RNA-binding protein Mex3b regulates the spatial organization of the Rap1 pathway. *Development (Cambridge, England)*, *141*(10), 2096–2107.

Leggett, B., & Whitehall, V. (2010). Role of the serrated pathway in colorectal cancer pathogenesis. *Gastroenterology*, *138*(6), 2088–2100.

Li, N., & Clevers, H. (2010). Coexistence of quiescent and active adult stem cells in mammals. *Science (New York, N.Y.)*, *327*(5965), 542–545.

Liang, J., Li, H., Han, J., Jiang, J., Wang, J., Li, Y., Feng, Z., Zhao, R., Sun, Z., Lv, B., & Tian, H. (2020). Mex3a interacts with LAMA2 to promote lung adenocarcinoma metastasis via PI3K/AKT pathway. *Cell Death & Disease*, *11*(8), 614.

Liu, Z., Dai, W., Jiang, L., & Cheng, Y. (2014). Over-expression of LGR5 correlates with poor survival of colon cancer in mice as well as in patients. *Neoplasma*, *61*(2), 177–185.

MacDonald, B. T., Tamai, K., & He, X. (2009). Wnt/beta-catenin signaling: components, mechanisms, and diseases. *Developmental Cell*, *17*(1), 9–26.

Makarova, K. S., Grishin, N. V., Shabalina, S. A., Wolf, Y. I., & Koonin, E. V. (2006). A putative RNA-interference-based immune system in prokaryotes: Computational analysis of the predicted enzymatic machinery, functional analogies with eukaryotic RNAi, and hypothetical mechanisms of action. *Biology Direct*, *1*(1), 1–26.

Mäkinen, M. J. (2007). Colorectal serrated adenocarcinoma. *Histopathology*, *50*(1), 131–150.

Maru, Y., Orihashi, K., & Hippo, Y. (2016). Lentivirus-Based Stable Gene Delivery into Intestinal Organoids. *Methods in Molecular Biology (Clifton, N.J.)*, *1422*, 13–21.

Matano, M., Date, S., Shimokawa, M., Takano, A., Fujii, M., Ohta, Y., Watanabe, T., Kanai,

T., & Sato, T. (2015). Modeling colorectal cancer using CRISPR-Cas9–mediated engineering of human intestinal organoids. *Nature Medicine*, *21*(3), 256–262.

Matia-González, A. M., Laing, E. E., & Gerber, A. P. (2015). Conserved mRNA-binding proteomes in eukaryotic organisms. *Nature Structural & Molecular Biology*, *22*(12), 1027–1033.

Mattiuzzi, C., Sanchis-Gomar, F., & Lippi, G. (2019). Concise update on colorectal cancer epidemiology. *Annals of Translational Medicine*, *7*(21), 609–609.

Mierzejewski, K., Paukszto, Ł., Kurzyńska, A., Kunicka, Z., Jastrzębski, J. P., Makowczenko, K. G., Golubska, M., & Bogacka, I. (2022). PPARγ regulates the expression of genes involved in the DNA damage response in an inflamed endometrium. *Scientific Reports*, *12*(1), 4026.

Mojica, F. J. M., Juez, G., & Rodriguez-Valera, F. (1993). Transcription at different salinities of Haloferax mediterranei sequences adjacent to partially modified PstI sites. *Molecular Microbiology*, *9*(3), 613–621.

Mundade, R., Imperiale, T. F., Prabhu, L., Loehrer, P. J., & Lu, T. (2014). Genetic pathways, prevention, and treatment of sporadic colorectal cancer. *Oncoscience*, *1*(6), 400–406.

Muñoz, J., Stange, D. E., Schepers, A. G., Van De Wetering, M., Koo, B. K., Itzkovitz, S., Volckmann, R., Kung, K. S., Koster, J., Radulescu, S., Myant, K., Versteeg, R., Sansom, O. J., Van Es, J. H., Barker, N., Van Oudenaarden, A., Mohammed, S., Heck, A. J. R., & Clevers, H. (2012). The Lgr5 intestinal stem cell signature: robust expression of proposed quiescent “+4” cell markers. *The EMBO Journal*, *31*(14), 3079–3091.

Pagano, J. M., Farley, B. M., Essien, K. I., & Ryder, S. P. (2009). RNA recognition by the embryonic cell fate determinant and germline totipotency factor MEX-3. *Proceedings of the National Academy of Sciences of the United States of America*, *106*(48), 20252–20257.

Panzeri, V., Manni, I., Capone, A., Naro, C., Sacconi, A., Di Agostino, S., de Latouliere, L., Montori, A., Pilozzi, E., Piaggio, G., Capurso, G., & Sette, C. (2021). The RNA-binding protein MEX3A is a prognostic factor and regulator of resistance to gemcitabine in pancreatic ductal adenocarcinoma. *Molecular Oncology*, *15*(2), 579–595.

Pereira, B., Amaral, A. L., Dias, A., Mendes, N., Muncan, V., Silva, A. R., Thibert, C., Radu, A. G., David, L., Máximo, V., van den Brink, G. R., Billaud, M., & Almeida, R. (2020). MEX3A regulates Lgr5+ stem cell maintenance in the developing intestinal epithelium. *EMBO Reports*, *21*(4).

Pereira, B., Billaud, M., & Almeida, R. (2017). RNA-Binding Proteins in Cancer: Old Players and New Actors. *Trends in Cancer*, *3*(7), 506–528.

Pereira, B., Le Borgne, M., Chartier, N. T., Billaud, M., & Almeida, R. (2013). MEX-3 proteins: recent insights on novel post-transcriptional regulators. *Trends in Biochemical Sciences*, *38*(10), 477–479.

Potten, C. S. (1977). Extreme sensitivity of some intestinal crypt cells to X and gamma irradiation. *Nature*, *269*(5628), 518–521.

Potten, C. S., Owen, G., & Booth, D. (2002). Intestinal stem cells protect their genome by selective segregation of template DNA strands. *Journal of Cell Science*, *115*(Pt 11), 2381–2388.

Powell, A. E., Wang, Y., Li, Y., Poulin, E. J., Means, A. L., Washington, M. K., Higginbotham, J. N., Juchheim, A., Prasad, N., Levy, S. E., Guo, Y., Shyr, Y., Aronow, B. J., Haigis, K. M., Franklin, J. L., & Coffey, R. J. (2012). The pan-ErbB negative regulator Lrig1 is an intestinal stem cell marker that functions as a tumor suppressor. *Cell*, *149*(1), 146–158.

Ran, F. A., Hsu, P. D., Wright, J., Agarwala, V., Scott, D. A., & Zhang, F. (2013). Genome engineering using the CRISPR-Cas9 system. *Nature Protocols*, *8*(11), 2281–2308.

Rodriguez-Bigas, M. A., Boland, C. R., Hamilton, S. R., Henson, D. E., Jass, J. R., Khan, P. M., Lynch, H., Perucho, M., Smyrk, T., Sobin, L., & Srivastava, S. (1997). A National Cancer Institute Workshop on Hereditary Nonpolyposis Colorectal Cancer Syndrome: meeting highlights and Bethesda guidelines. *Journal of the National Cancer Institute*, *89*(23), 1758–1762.

S. Srivastava, A., B. Singh, A., Ahmad, R., & Dhawan, P. (2011). Cancer stem cells and colorectal cancer: an overview. *Current Topics in Medicinal Chemistry*, *11*(13), 1592–1598.

Sangiorgi, E., & Capecchi, M. R. (2008). Bmi1 is expressed in vivo in intestinal stem cells. *Nature Genetics*, *40*(7), 915–920.

Sato, T., Stange, D. E., Ferrante, M., Vries, R. G. J., Van Es, J. H., Van Den Brink, S., Van Houdt, W. J., Pronk, A., Van Gorp, J., Siersema, P. D., & Clevers, H. (2011). Long-term expansion of epithelial organoids from human colon, adenoma, adenocarcinoma, and Barrett's epithelium. *Gastroenterology*, *141*(5), 1762–1772.

Sato, T., Van Es, J. H., Snippert, H. J., Stange, D. E., Vries, R. G., Van Den Born, M., Barker, N., Shroyer, N. F., Van De Wetering, M., & Clevers, H. (2011). Paneth cells constitute the niche for Lgr5 stem cells in intestinal crypts. *Nature*, *469*(7330), 415–418.

Sato, T., Vries, R. G., Snippert, H. J., Van De Wetering, M., Barker, N., Stange, D. E., Van Es, J. H., Abo, A., Kujala, P., Peters, P. J., & Clevers, H. (2009). Single Lgr5 stem cells build crypt-villus structures in vitro without a mesenchymal niche. *Nature*, *459*(7244),

262–265.

Sauer, B. (1998). Inducible gene targeting in mice using the Cre/lox system. *Methods (San Diego, Calif.)*, *14*(4), 381–392.

Schatoff, E. M., Leach, B. I., & Dow, L. E. (2017). Wnt Signaling and Colorectal Cancer. *Current Colorectal Cancer Reports*, *13*(2), 101–110.

Shimokawa, M., Ohta, Y., Nishikori, S., Matano, M., Takano, A., Fujii, M., Date, S., Sugimoto, S., Kanai, T., & Sato, T. (2017). Visualization and targeting of LGR5+ human colon cancer stem cells. *Nature*, *545*(7653), 187–192.

Simons, B. D., & Clevers, H. (2011). Stem cell self-renewal in intestinal crypt. *Experimental Cell Research*, *317*(19), 2719–2724.

Sun, Z., Yu, X., Wang, H., Zhang, S., Zhao, Z., & Xu, R. (2014). Clinical significance of mismatch repair gene expression in sporadic colorectal cancer. *Experimental and Therapeutic Medicine*, *8*(5), 1416–1422.

Sung, H., Ferlay, J., Siegel, R. L., Laversanne, M., Soerjomataram, I., Jemal, A., & Bray, F. (2021). Global Cancer Statistics 2020: GLOBOCAN Estimates of Incidence and Mortality Worldwide for 36 Cancers in 185 Countries. *CA: A Cancer Journal for Clinicians*, *71*(3), 209–249.

Takeda, N., Jain, R., LeBoeuf, M. R., Wang, Q., Lu, M. M., & Epstein, J. A. (2011). Interconversion between intestinal stem cell populations in distinct niches. *Science (New York, N.Y.)*, *334*(6061), 1420–1424.

Thompson, S. L., Bakhoum, S. F., & Compton, D. A. (2010). Mechanisms of chromosomal instability. *Current Biology*, *20*(6), R285–R295.

Van De Wetering, M., Francies, H. E., Francis, J. M., Bounova, G., Iorio, F., Pronk, A., Van Houdt, W., Van Gorp, J., Taylor-Weiner, A., Kester, L., McLaren-Douglas, A., Blokker, J., Jaksani, S., Bartfeld, S., Volckman, R., Van Sluis, P., Li, V. S. W., Seepo, S., Sekhar Pedamallu, C., … Clevers, H. (2015). Prospective derivation of a living organoid biobank of colorectal cancer patients. *Cell*, *161*(4), 933–945.

Van Der Flier, L. G., & Clevers, H. (2009). Stem cells, self-renewal, and differentiation in the intestinal epithelium. *Annual Review of Physiology*, *71*, 241–260.

van der Flier, L. G., Haegebarth, A., Stange, D. E., van de Wetering, M., & Clevers, H. (2009). OLFM4 is a robust marker for stem cells in human intestine and marks a subset of colorectal cancer cells. *Gastroenterology*, *137*(1), 15–17.

van der Flier, L. G., van Gijn, M. E., Hatzis, P., Kujala, P., Haegebarth, A., Stange, D. E., Begthel, H., van den Born, M., Guryev, V., Oving, I., van Es, J. H., Barker, N., Peters,

P. J., van de Wetering, M., & Clevers, H. (2009). Transcription factor achaete scute-like 2 controls intestinal stem cell fate. *Cell*, *136*(5), 903–912.

Van Es, J. H., Jay, P., Gregorieff, A., van Gijn, M. E., Jonkheer, S., Hatzis, P., Thiele, A., van den Born, M., Begthel, H., Brabletz, T., Taketo, M. M., & Clevers, H. (2005). Wnt signalling induces maturation of Paneth cells in intestinal crypts. *Nature Cell Biology 2005 7:4*, *7*(4), 381–386.

VanDussen, K. L., Carulli, A. J., Keeley, T. M., Patel, S. R., Puthoff, B. J., Magness, S. T., Tran, I. T., Maillard, I., Siebel, C., Kolterud, Å., Grosse, A. S., Gumucio, D. L., Ernst, S. A., Tsai, Y. H., Dempsey, P. J., & Samuelson, L. C. (2012). Notch signaling modulates proliferation and differentiation of intestinal crypt base columnar stem cells. *Development (Cambridge, England)*, *139*(3), 488–497.

Vousden, K. H., & Prives, C. (2009). Blinded by the Light: The Growing Complexity of p53. *Cell*, *137*(3), 413–431.

Walther, A., Johnstone, E., Swanton, C., Midgley, R., Tomlinson, I., & Kerr, D. (2009). Genetic prognostic and predictive markers in colorectal cancer. *Nature Reviews Cancer 2009 9:7*, *9*(7), 489–499.

Willert, K., Brown, J. D., Danenberg, E., Duncan, A. W., Weissman, I. L., Reya, T., Yates, J. R., & Nusse, R. (2003). Wnt proteins are lipid-modified and can act as stem cell growth factors. *Nature*, *423*(6938), 448–452.

Yan, K. S., Janda, C. Y., Chang, J., Zheng, G. X. Y., Larkin, K. A., Luca, V. C., Chia, L. A., Mah, A. T., Han, A., Terry, J. M., Ootani, A., Roelf, K., Lee, M., Yuan, J., Li, X., Bolen, C. R., Wilhelmy, J., Davies, P. S., Ueno, H., … Kuo, C. J. (2017). Non-equivalence of Wnt and R-spondin ligands during Lgr5+ intestinal stem-cell self-renewal. *Nature*, *545*(7653), 238–242.

Yang, Y., Wang, S. Y., Huang, Z. F., Zou, H. M., Yan, B. R., Luo, W. W., & Wang, Y. Y. (2016). The RNA-binding protein Mex3B is a coreceptor of Toll-like receptor 3 in innate antiviral response. *Cell Research*, *26*(3), 288–303.

Yao, Y., Xu, X., Yang, L., Zhu, J., Wan, J., Shen, L., Xia, F., Fu, G., Deng, Y., Pan, M., Guo, Q., Gao, X., Li, Y., Rao, X., Zhou, Y., Liang, L., Wang, Y., Zhang, J., Zhang, H., … Hua, G. (2020). Patient-Derived Organoids Predict Chemoradiation Responses of Locally Advanced Rectal Cancer. *Cell Stem Cell*, *26*(1), 17-26.e6.

Zheng, H., Liu, H., Li, H., Dou, W., Wang, J., Zhang, J., Liu, T., Wu, Y., Liu, Y., & Wang, X. (2022). Characterization of stem cell landscape and identification of stemness-relevant prognostic gene signature to aid immunotherapy in colorectal cancer. *Stem Cell Research and Therapy*, *13*(1), 1–20.

Zhong, Z. A., Michalski, M. N., Stevens, P. D., Sall, E. A., & Williams, B. O. (2021).

Regulation of Wnt receptor activity: Implications for therapeutic development in colon cancer. *Journal of Biological Chemistry*, *296*, 100782.

Ziskin, J. L., Dunlap, D., Yaylaoglu, M., Fodor, I. K., Forrest, W. F., Patel, R., Ge, N., Hutchins, G. G., Pine, J. K., Quirke, P., Koeppen, H., & Jubb, A. M. (2013). In situ validation of an intestinal stem cell signature in colorectal cancer. *Gut*, *62*(7), 1012–1023.

Appendix A | List of primers and antibodies used in this study.

PRIMER SEQUENCES (5'-3')

	Forward	Reverse
Lgr5	AGCGTCTTCACCTCCTACCTG	CTTGGGAATGTGTGTCAAAGC
Axin2	AGCGTCTTCACCTCCTACCTG	TTTGGCTCTTTGTGATCTTCTGG
Lrig1	CAAGCTGACTCTGTTTGGAAAC	ACTGGACAGACCTGATTGC
Angptl4	ATCTTCAGAGCCAGATAGACC	AGCTGGGTCATCTTGGGAAG
Pcna	GGGCTGAAGATAATGCAGACA	TGTACTCCTGTTCTGGGATTC
18S	CGCCGCTAGAGGTGAAATTC	CATTCTTGGCAAATGCTTTCG

ANTIBODIES

Antigen	Application*	Description	Dilution	Source
Ki67	IHC	Rabbit monoclonal (SP6)	1:2000	Abcam (ab197547)
PPARγ	IHC and WB	Rabbit monoclonal	1:600 (IHC); 1:1000 (WB)	Cell Signaling Technology (C26H12)
Keratin-20	IHC	Rabbit monoclonal	1:750	Cell Signaling Technology (D9Z1Z)
β-catenin	IHC and WB	Mouse monoclonal	1:1000 (IHC and WB)	BDBiosciences (610153)
MEX3A	WB	Rabbit polyclonal	1:2000	Sigma-Aldrich (PRS4869)
p53	IHC	Mouse monoclonal	1:375 (IHC) 1:500 (WB)	Thermo Fisher Scientific (PAb240)
β-actin	WB	Mouse monoclonal	1:4000	Santa Cruz Biotech (SC-47778)
Hs- LGR5	ISH	RNA probes	-	Advanced Cell Diagnostics (311021)
Hs-MEX3A	ISH	RNA probes	-	Advanced Cell Diagnostics (555741)
Secondary				
Goat anti-mouse IgG	WB	HRP-linked Antibody	1:3000	Sigma-Aldrich (A5278)
Goat anti-rabbit IgG	WB	HRP-linked Antibody	1:10000	Cell Signaling Technology (7074)

* IHC: immunohistochemistry; ISH: In situ hybridization; WE: Western-Blot